2011

Emission Enhancement Through Dual Donor Sensitization And Photo-Luminescine Properties Of Europium(Iii)And Terbium(Iii) -Terpyridine -Tetracyanoplatinate Complexes

Nuquie Glekeh Beedoe
North Carolina Agricultural and Technical State University

EMISSION ENHANCEMENT THROUGH DUAL DONOR SENSITIZATION AND PHOTO-LUMINESCINE PROPERTIES OF EUROPIUM(III) AND TERBIUM(III) -TERPYRIDINE – TETRACYANOPLATINATE COMPLEXES

by

Nuquie Glekeh Beedoe

A thesis submitted to the graduate faculty
in partial fulfillment of the requirements for the degree of
MASTER OF SCIENCE

Department: Chemistry
Major: Chemistry
Major Professor: Dr. Zerihun Assefa

North Carolina A&T State University
Greensboro, North Carolina
2011

School of Graduate Studies
North Carolina Agricultural and Technical State University

This is to certify that the Master's Thesis of

Nuquie Glekeh Beedoe

has met the thesis requirements of
North Carolina Agricultural and Technical State University

Greensboro, North Carolina
2011

Approved by:

Dr. Zerihun Assefa Major Professor	Dr. Alex Williamson Committee Member
Dr. Mufeed Basti Committee Member	Dr. Margaret Kanipes Department Chairperson

Dr. Sajiv Sarin
Dean of Graduate Studies

DEDICATION

This thesis is dedicated to Janneh Peters-Beedoe and Nuquie Glekeh Beedoe Jr.

BIOGRAPHICAL SKETCH

Nuquie Glekeh Beedoe was born on February 1, 1981, in Gbarnga, Liberia. He moved to the United States of America on November 27, 1997. He obtained his high school education at Robert B. Glenn High School in Kernersville, North Carolina in 2001. He achieved the Bachelor of Science degree in Chemistry from North Carolina Agricultural and Technical State University in 2006. He is a candidate for the Master of Science degree in Chemistry.

ACKNOWLEDGEMENTS

I would like to take this opportunity and give thanks to God for providing me life, strength, and good health. Tremendous thanks to Dr. Zerihun Assefa for his time, guidance and knowledge that were invested in me while conducting my studies. I would like to give thanks to Dr. Assefa's research group – Darkus Elizabeth Jenkins, Carlos Crawford, Kendra Whitehead, and Matthew Mickens. Thanks to my thesis advisory committee members Dr. Alex Williamson and Dr. Mufeed Basti. Thanks to Ms. Carolyn Mayo and the Department of Chemistry, faculty and staff. I would like to extend my appreciation and thanks to Dr. Richard Sykora of the University of Southern Alabama for providing crystals which were used in accomplishing the luminescence studies. I would like to give special thanks to my parents Dr. Shelton Beedoe and Joan Slocum. Love and thanks go to my wife Janneh Peters-Beedoe for supporting me in accomplishing my goal as a graduate student. Thanks to my son Nuquie Glekeh Beedoe Jr for bringing me peace, joy and making me smile. This project was partly supported by the NOAA Educational Partnership Program award number NA06OAR4810187 to NCAT State University , and donors of the American Chemical Society -Petroleum Research Fund (ACS-PRF).

TABLE OF CONTENTS

LIST OF FIGURES

FIGURES **PAGE**

LIST OF TABLES

TABLES **PAGE**

LIST OF SYMBOLS

UV	Ultraviolet
S_0	Ground Singlet State
Terpy	Terpyridine
IET	Intermolecular Energy Transfer
nm	nanometer
g	gram
NMR	Nuclear Magnetic Resonance
NIR	Near-Infrared
cm	Centimeter
CPL	Circularly Polarized Luminescence
Bpy	2, 2′-bipyridine
MLCT	Metal to Ligand Charge Transfer
Phterpy	4′-phenylethnyl-2, 2′:6′, 2″-terpyridine
TCP	Tetracynoplatinates
a. u.	Arbitrary Unit

ABSTRACT

Beedoe, Nuquie Glekeh. EMISSION ENHANCEMENT THROUGH DUAL DONOR SENSITIZATION AND PHOTO-LUMINESCINE PROPERTIES OF EUROPIUM(III) AND TERBIUM(III) -TERPYRIDINE -TETRACYANOPLATINATE COMPLEXES. **(Major Advisor: Zerihun Assefa)** North Carolina Agricultural and Technical State University.

Luminescence studies were conducted on tetracyanoplatinate complexes that contain up to four different ligands simultaneously, resulting in very complex structural features. Most of the complexes of (terpy)-Eu-platinum tetra cyanide complexes (terpy = terpyridine) crystallize with low one-, and two-dimensional structural types. The effects of anion variation on the intermolecular energy transfer (IET) mechanism are discussed in detail. Temperature dependent luminescence studies were also conducted on terbium based compounds that contain different ligands resulting in complex structural features. The system also displays dual donor feature where both the organic ligand (terpyridine) and the platinum tetracyanide (TCP) metal complex act as donors. When the counter anion is changed to the acetate ion, the bonding interaction between the donor (TCP complex) and acceptor (Eu^{3+} and Tb^{3+}) is removed, and the energy transfer pathway is blocked. As a result, the donor emits strongly, albeit totally quenched in the complexes with direct bonding interaction. Moreover, all of these complexes show interesting structural features that consist of channels capable of accommodating volatile organic compounds (VOC). Studies on VOC sensing by these compounds is currently in progress in our laboratory. Details of the photoluminescence studies are presented in this thesis.

CHAPTER 1

INTRODUCTION

1.1. Luminescence Theory

Luminescence is defined as the emission of light from an excited electronic state of a molecular species [1-3]. Luminescence occurs when an electron returns to the electronic ground state from an excited state and loses its excess energy as a photon [2].

There are several types of luminescence spectroscopic techniques. Some of these techniques include molecular fluorescence, phosphorescence, and chemiluminescence [2, 4]. Fluorescence and phosphorescence are comparable in that excitation is brought about by absorption of photon [4]. Together fluorescence and phosphorescence are referred to as photoluminescence [4]. Fluorescence takes a shorter time to occur compared to phosphorescence. The lifetime for fluorescence is usually in the order of nanoseconds or less and phosphorescence is on the order of micro seconds to longer time [1]. These lifetimes vary depending on the system under study. Fluorescence takes place when a molecule absorbs UV radiation. As a result the vibrational level in the electronic ground state is excited to the excited singlet state [2]. In contrast to fluorescence and phosphorescence, chemiluminescence occurs when a chemical reaction produces an electronically excited species which emits a photon when it falls to the ground state [1, 2].

To better understand the luminescence process the energy diagram shown in Figure 1.1 is used. The ground singlet state (S_0) is a molecular electronic state in which

all electron spins are paired and no splitting of electronic energy levels occurs when the molecule is exposed to a magnetic field [4]. A singlet or triplet excited state occurs when one pair of a molecule is excited to a higher energy level [1, 2, 4, 5]. The spin of the singlet excited state is still paired with the ground state when promotion of electron occurs [1, 2, 4, 5]. However, in the triplet state the spins of the two electrons become parallel [1, 2, 4, 5]. These trends follow the Pauli Exclusion Principle which states that two electrons in an atom are not allowed to have the same set of the four quantum numbers [4]. As a result of this rule, a maximum of two electrons can occupy a molecular orbital with opposite spin.

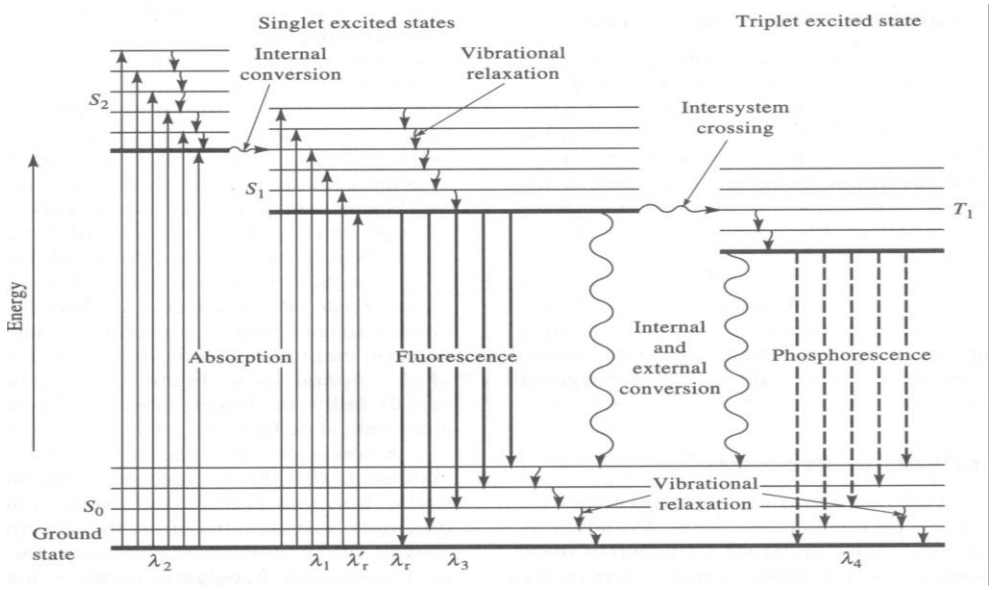

Figure 1.1. Jablonski's diagram showing the photoluminescence system [6].

The ground state represented by S_0 is normally a singlet state and S_1 and S_2 represent the first and second electronic singlet states, respectively [4]. The triplet state is represented by T_1.When light is absorbed by the molecule an electron is promoted within $10^{-14} – 10^{-15}$ s from the ground electronic state to an excited state that should possess the same spin multiplicity as the ground state [1].

Internal conversion is a non-radiative relaxation processes that occurs between electronic states of like spin multiplicity such as S_1 to S_2 [1]. This process is most efficient when the electronic energy levels are sufficiently close so that the vibrational energy levels overlap [4]. Another non-radiative relaxation process is the intersystem crossing. In this process relaxation occur between excited states of different spin multiplicities [1]. The spin of an excited electron is reversed and a change in multiplicity of the molecule results in an intersystem crossing process.

1.2. Chemistry of Europium and Terbium

The study focuses on the luminescence properties of the rare-earth element (lanthanide series). Europium and terbium were two of elements that were studied in this research; these brief introductions regarding these metals will be presented. They both have some similar properties and usage because of their location on the periodic table. Both belong to the rare-earth elements (lanthanide series) [7]. In common with other lanthanides, both elements are found mostly in the minerals monazite, bastnasite, cerite, and allanite[8]. An attractive feature of luminescent lanthanide compounds is their line-like emission, which results in a high color purity of the emitted light [8]. Europium (III)

and terbium (III) are used as luminescent probes, stains for biomolecular systems and as alternative for conventional organic based fluorescent probes [9, 10].

Europium was spectroscopically discovered in 1901 by Eugene-Anatole Demarcay (1852-1904) [7]. He was the first to separate it from the rare-earth samarium [7]. The element was named after the continent Europe. It has two stable naturally occurring isotopes which are europium-151 and europium-153. Europium is a soft steel-gray, very soft metal that is difficult to prepare [7].

Europium has a similar chemistry to that of the group 2 elements calcium, strontium, and barium [7]. In air europium oxidizes rapidly and will react with water to release hydrogen [7]. The element can be found in most of the rare-earth ores and is the fiftieth most abundant element on earth [6]. The typical method of preparation is by heating europium (III) oxide with excess lanthanum under vacuum. Europium is used as a neutron absorber in nuclear reactors, to add red color to TV tubes, and as an addition to the glue on postage stamps so they can be read electronically [8]. Example of a common europium compound is europium oxide (Eu_2O_3) that is used to make infrared-sensitive phosphors and as nuclear reactor control rods. Biologically europium has no known role and it has low toxicity.

The main oxidation states of europium are Eu^{+3} and Eu^{+2}. There have been studies done on europium complexes in the +3 oxidation state with coordination numbers six, seven, eight, nine, and ten [11]. The narrow f-f transitions allowed a good sensitization of the Eu^{+3} luminescence through the antenna effect [11]. Europium metal is very reactive

and may burst into flames spontaneously at room temperature when it is in the form of powder [8].

Terbium is the other lanthanide metal that was studied during this research. The metal terbium was discovered in 1843 in Stockholm, Sweden by Carl Gustaf Mosander (1797-1858). Mosander discovered several rare-earth elements in addition to terbium, which was named for one of the syllables of Ytterby, a stone quarry in Sweden where many of the rare-earths were first found [8]. Terbium is a member of the group 11 rare-earth elements. It has no stable isotopes, where 159 Tb makes up 100% of the natural element. Terbium is a very reactive, silver-gray metallic element found in the yttrium subgroup (lanthanide series) of the rare-earths [8].

Terbium reacts slowly in air at room temperature but will burn at higher temperatures and shows the normal metallic property of being ductile and malleable [8]. It is the fifty-seventh most abundant element on earth [6]. Terbium is usually found in the compound form compared to the free metal. Examples of common compounds of terbium are terbium nitrate $Tb(NO_3)_3$ which is used as activator for solid state devices and terbium oxide (Tb_2O_3) which is a brown powder that absorbs carbon dioxide [8]. Other usage of terbium includes the activation of the phosphors for TV picture tubes and controlling rods of nuclear reactors.

1.3. Application of Lanthanide

The luminescence properties of lanthanide make them interesting candidates for many applications. Their emission mechanism is based on f-f transitions with consequent

narrow emission bands that enable them to be used in label technology for clinical diagnostic [12, 13]. The f-f transitions are spin and parity forbidden, but when coordinated to ligands their sensitized emission can be utilized [12]. Lanthanide ions have many interesting light-emission properties due to their f-f transitions [14]. Among the lanthanide ions, Eu^{+3} and Tb^{+3} possess good luminescence characteristics based on the 4f electronic transitions [15]. As a result of these properties, lanthanides can be used in applications such as phosphors, in biomedical field (as sensors, and in imaging), fluoroimmunoassays, X-ray detectors, fluorescent tubes, and liquid-crystalline displays [12, 15-18]. Lanthanide ions have been used to probe many structural and analytical problems such as the determination of local symmetries in crystalline inorganic materials, catalysis, probing the structure of biological macromolecules, and immunoassays using time-resolved luminescence [1]. Lanthanides have many uses in inorganic systems; for example, they can be used with pure or doped solids of oxides and inorganic salts in order to understand the molecular and electronic structures of these systems, or to assess their potential use as a solid-state photonic device [1]. Among the lanthanides europium(III) and terbium(III) are attractive luminescent materials with many important applications including lasers, phosphors, projection television screens and optical communication amplifiers [16, 19, 20].

The fascinating optical and magnetic properties of lanthanide ions have promoted the use of their complexes in an increasing number of technological applications ranging from biomedical analysis (fluoroimmunoassays, MRI contrast agents, and cellular imaging) to materials science (lasers, optical fibers, light emitting diodes, optical

displays, and electron luminescent devices) [18, 21-24]. Lanthanide ions have sharp characteristic emission in the visible and near-infrared (NIR) ranges, long luminescence lifetime, light-conversion material, and large Stokes shift, which makes them very attractive candidates for the development of optical devices [21, 24]. Ligands that are comprised of strongly absorbing chromophores can be conveniently used to sensitize lanthanide emission at low energy [21]. Ln(III) organic ligand complexes (Ln = Eu and Tb especially) offer a number of advantageous features as fluorescent labels over conventional organic dyes [22]. These advantages include (1) long emission lifetimes under ambient conditions, (2) no self-quenching, and (3) excellent solubility in water [22].

The coordination chemistry of lanthanides pertains to the exploitation of their trivalent ions in biology and medicine. Several research themes have been developed including the design of time-resolved fluoroimmunoassys, the labeling and specific cleavage of DNA and RNA, the synthesis of efficient shift reagents for NMR spectroscopy and contrast agents for nuclear magnetic imaging, and the development of photosensitizers for cancer therapy [25]. The presence of unpaired electrons grant them paramagnetic properties used for structural determination in solution or for the development of contrast agents in MRI [26]. Additional, lanthanides can be used in nuclear medicine for both diagnosis and therapy because of their radioactive isotopes [26].

1.4. Luminescence Studies of Europium and Terbium

Among the lanthanide ions, Eu^{+3} and Tb^{+3} possess efficient luminescence characteristics based on the 4f electronic transitions [15]. These lanthanides possess good luminescence properties based on their electronic transitions between the 4f energy levels [27]. However, since the f-f transitions of these cations are forbidden, the intensity of absorption bands are usually weaker [14, 15, 18, 27, 28]. On the other hand, photoactive lanthanide organic coordinate compounds usually exhibit extensive luminescence due to the strong absorption of the ligands in the ultraviolet region and efficient energy transfer from the ligands to the central lanthanide ions [15]. These ions exhibit intense narrow band emission when combined with β-diketone, aromatic carboxylic acids and heterocyclic ligands [15, 27, 29].

Studies on gels codoped with terbium and phenathroline shows excitation spectrum that exhibits a very broad band ranging from 250 nm to 400 nm with the maximum excitation wavelength centered at 330 nm [15]. The characteristic transitions of Tb^{+3} ($^5D_4 \rightarrow {}^7F_J$, J = 6, 5, 4, 3) is seen in the complexes of gels codoped with terbium, Langmuir-Blodgett films, phenathroline and polyvinyl alcohol (PVA) films, with the $^5D_4 \rightarrow {}^7F_5$ as the dominant transition [13, 24, 30, 31]. The emission intensity of the gel codoped with terbium and phenathroline shows an approximate 30% fluorescence value of the pure terbium complex powder and 45 times stronger than that of the gel doped separately with terbium, suggesting that an efficient energy transfer takes place from phenathroline to central terbium ion Tb^{+3} [15]. The gel that was codoped with europium and phenathroline shows a very broad band instead of the narrow absorption band of Eu^{+3}

usually appearing at around 395 nm. Energy transfer from phenathroline to Eu^{+3} is demonstrated by the luminescence intensity of the gel codoped with europium and phenathroline which is more than 50 times larger than the gel doped only with europium [15].

The advantages of complexes with Eu^{+3} and Tb^{+3} are their high photoluminescence efficiency, and sharp emission spectrum along with their strong binding and chromophoric domain [19, 22]. Ln(III) ions due to their unique luminescence properties, such as long luminescence decay time and narrow emission bands can form highly luminescent complexes with several groups of ligands [32]. When these cations are incorporated into the same polymer backbone, changes in the luminescence spectrum occurs, yielding a yellow color emission [19]. When the polymers were complexed with Eu^{+3} or Tb^{+3}, production of pink and green color was emitted respectively [19].

Luminescence spectroscopy of europium and terbium are commonly used in the study of biomolecular structure. Studies involving the luminescence of metal ions in biomolecular structure have been limited because the metal ions known to be essential or important to biological structure and function has no luminescent under biological conditions [9]. Exceptions to this nonluminescent behavior of metal ions are trivalent Eu^{+3} and Tb^{+3}. Both Eu^{+3} and Tb^{+3} are luminescent in aqueous solution, and both generally retain their luminescence when bound to complex ligand systems [9]. Additionally, they exhibit numerous emissions due to several electronic transitions whose relative intensities and line splitting patterns are sensitive to the detailed nature of the ligand environment about the metal ion [9].

There are certain conditions that enable Eu^{+3} and Tb^{+3} to be used as luminescent probes of metal binding in biomolecular system. These conditions include but may not be limited to (1) their coordination chemistry must be compatible with the metal ion binding properties of the system to be studied and (2) their binding properties must exhibit some degree of site selectivity [9]. The binding preference of donor atoms most commonly found in biomolecular systems are O > N > S, due to the fact that europium and terbium are both hard acids in the Pearson classification scheme [9]. The coordination of europium and terbium normally occurs predominately via ionic bonding interactions, leading to a strong preference for negatively charged donor groups that are also hard bases [9]. Europium and terbium complexes exhibit coordination numbers ranging from six to twelve, with eight and nine being the most common [9]. With respect to Eu^{+3} and Tb^{+3} binding to biomolecular systems, the following points are of special importance: (1) site selectivity, (2) size and geometry of binding sites, (3) binding strength, and (4) site distortions [9]. Recent interest in Eu^{+3} and Tb^{+3} ions as biomolecular structure probes has focused on their use as replacement probes for Ca^{+2} and Mg^{+2} in few cases [9, 33]. The substitution of Eu^{+3} and Tb^{+3} into biological systems that contain Ca^{+2} and Mg^{+2} can lead to exploiting the spectroscopic properties of the ions for obtaining information on the structural features of Ca^{+2} and Mg^{+2} biochemistry [9].

For europium (III) complexes in aqueous solution, all emission originates from the nondegenerate $^5D_0$ level when excitation is at 578 nm [9]. The strongest emissions are always observed in the $^5D_0 \rightarrow {}^7F_1$ and $^7F_2$ transition regions, and $^5D_0 \rightarrow {}^7F_4$ emission is frequently observed to have a moderately strong intensity [9, 16, 34]. When europium

(III) complexes are in nonaqueous solutions, it is often possible to observe emissions from the $^5D_1$ and $^5D_2$ levels when excitation is at 523 nm or 465 nm respectively [9]. The most important Eu^{+3} excitation mode involve direct excitation of the $^5D_0$ emitting level via the $^7F_0 \rightarrow {}^5D_0$ absorptive transition are $^5D_0 \rightarrow {}^7F_{1,2}$ along with the $^5D_0 \rightarrow {}^7F_3$ and $^5D_0 \rightarrow {}^7F_4$ transitions [9, 16, 18, 24, 33].

For terbium (III) complexes in aqueous solution, essentially all emissions emanate from the $^5D_4$ level when excitation is at 20400 cm^{-1} [9]. Emission can be seen in each of the $^5D_4 \rightarrow {}^7F_J$ (J = 0, 1, 2, 3, 4, 5, or 6) transition regions, but invariably the most intense emission is observed in the $^5D_4 \rightarrow {}^7F_5$ transition region [9, 30, 31]. The $^5D_4 \rightarrow {}^7F_{0,1}$ emissions are always weak, and the relative intensities of the remaining emission fall in the order $^5D_4 \rightarrow {}^7F_6 > {}^7F_4 > {}^7F_3 > {}^7F_2$ [9, 30, 31, 33]. Among the Tb^{+3} transitions, $^5D_4 \rightarrow {}^7F_5$ is the best probe transition.

When the ligand environment about either Eu^{+3} or Tb^{+3} is chiral or contains chiral centers, the $^5D_J \rightarrow {}^7F_J$ transitions contains unequal amounts of left- and right-circularly polarized light [9]. This phenomenon is generally referred to as either emission optical activity or circularly polarized luminescence (CPL) [9, 28]. The luminescent chromophores most commonly found in biomolecular system generally exhibit broad-band luminescence spectra falling within the 280-500 nm (35,700-20000 cm^{-1}) [9]. Examples of these chromophores include the nucleic acid bases, the tryptophan, tyrosine, and phenylalanine amino acid residues in protein.

1.5. Terpyridine as a Ligand

The ligand terpy is used in the process of reversible luminescence switching in metals when it replaces 2,2′-bipyridine (bpy) [35]. Excitation of the complex by means of the characteristic metal-to-ligand charge-transfer (MLCT) absorption band produces an excited triplet state in which the promoted electron is localized on the terpyridine ligand. Substitution of the bipy with terpy is a way to eliminate the introduction of enantiomers, allowing the use of rigid or geometrically constrained linkers [35]. The complex $[Ru(terpy)_2]^{+2}$ is nonluminescent at room temperature, but this problem can be overcome by proper functionalization of the coordination sphere around the cation [35]. Visible light illumination causes charge transfer from the metal center to the acetylene-bearing terpy ligand when one of the other ligand is replaced with 4′-phenylethnyl-2,2′:6′,2″-terpyridine (phterpy) [35]. As a result the triplet lifetime is enhanced significantly [35].

Terpy ligand is seen in the process of intermolecular energy transfer in molecular dye comprising free-base porphyrin and ruthenium(II) bis(terpy) termini, and organometallic platinum (II) terpy [36, 37]. The metals bis(terpy) complexes are also used in the applications of modules for construction of linear arrays and bridge for porphyrin based triads [36]. The triplet lifetime of ruthenium(II) bis(terpy) is too short to be used for the complex to be a useful sensitizer or energy relay [36]. The triplet lifetime of these complexes are greatly enhanced by the substitution of an alkynylene group at the 4′-position of the terpyridyl ligand [36]. These metal complexes are linked directly to the porphyrin ring via the meso-position [36]. When terpy ligand is attached to an alkyne substituent, the net result is that the triplet lifetime of the ruthenium(II) bis(2,2′:6′,2″-

terpyridine) subunit is prolonged to such an extent that this species operates as an energy relay [38]. Intermolecular energy transfer also occurs from a free-base porphyrin to an attached osmium(II) bis(terpy) complex [38]. The approach involves plused excitation of a porphyrin that is covalently attached to an Os(II) bis(terpy) by way of a short spacer [38]. The singlet excited state of the porphyrin produced upon illumination transfer the excitation energy to the metal complex on a very fast time scale so as to generate the MLCT triplet state within a few picoseconds [38]. When the electron is promoted, it resides on the proximal terpy ligand [38]. In contrast with the corresponding Ru(II) and Os(II) complexes, bis(terpy)iron(II) does not emit following excitation to the MLCT excited state [39]. Instead, the MLCT excited state undergoes rapid intersystem crossing to form the long-lived $^5T_2$ ligand-field excited state [39].

In addition to the terpy ligand being used by metals separately, intermolecular electron exchange in mixed-metal Ru^{II}-Os^{II} polypyridyl assemblies system and Pt(II)-polypyridine complexes have also been study [37, 40]. The system is convenient because of the favorable thermodynamically energy passage from Ru^{II} to Os^{II} [40]. Energy transfer occurs with high efficiency from the Ru(II) units to the Os(II) center at all temperature [40]. Ruthenium(II) bis(terpy)-based (Ru-terpy) terminals act as energy donors for the central osmium(II) bis(terpy)-based (Os-terpy) core [40]. The acceptor complex is known to emit in fluid solution at room temperature, thereby facilitating the study of intermolecular excitation energy redistribution [40].

The absorption spectrum of the Ru(II) and Os(II) metal complex in acetonitrile at room temperature displays the characteristic bands associated with bis(terpy) complexes

containing Os(II) and Ru(II) metal centers [40]. The spectra show a broad absorption band canter around 500 nm which is assigned to the metal-to-ligand charge transfer (MLCT) absorption bands for the Ru-terpy and Os-terpy units [40]. The spin-forbidden MLCT transitions associated with the Os-terpy can be seen as the low intensity tail [40]. Broad luminescence band which is centered around 750 nm is the result of excitation into the 500 nm peak [40]. This emission profile and position are similar to those found for related Os-terpy derivatives [40]. There is no indication of emission from the Ru-terpy unit, which is expected around 675 nm. The excitation spectrum is a good match with the absorption spectrum over the entire spectral region [40]. As a result, the assumption can be made that energy transfer from Ru-terpy to Os-terpy is efficient in the target compound [40].

Emission from Os-terpy is unaffected by presence of the second metal as shown by the comparison of the photophysical properties recorded for the Os-terpy and Ru-terpy center present in the complex [40]. The yield and lifetime for emission localized on the Ru-terpy canter are heavily quenched at all temperatures. The overall system is consistent with efficient intermolecular triplet energy transfer to the central Os-terpy unit [40]. There was also a triplet energy transfer found for the system when it was conducted in a frozen butyronitrile glass using excitation at 480 nm with a 4 ns laser pulse [40]. At low temperature in the glassy matrix, the limiting rate of energy transfer is set by Forster-type dipole-dipole interactions [40]. In contrast, at higher temperature, Dexter-type electron exchange takes place via a weakly activated process. In addition to the frozen glass, there was also triplet energy transfer found in fluid solution [40].

The photophysical properties of Eu^{3+} marocyclic receptors containing a terpyridine moiety as part of a polyamine ring with N-pendant acetate groups have been studied [22]. The terpyridine group is a suitable energy-absorbing and energy-transferring moiety, as a result, it act as photosensitizer antenna to improve the luminescence of Eu^{3+} ion in biological media [22]. The lowest excited state of the terpyridine (E ($^3\pi\pi^*$) = 23000 cm^{-1}) is sufficiently high in energy to be able to transfer excitation to the luminescence levels of Eu^{3+} ion (^5D_J, J = 0-2) [22]. The complexes of Eu(III) in aqueous media gave europium-centered luminescence spectra, with the strongest transition at 620 nm ($^5D_0 \rightarrow {}^7F_2$ transition) when photoexcited in the lowest energy absorption of the heterocyclic chromophore [22]. The transfer of energy from the excited states of the ligand to the Eu(III) emission states is shown by the similarity between the excitation and absorption spectra of the complexes [22].

Emission from the f-f transitions of Eu^{3+} is observed for Eu-terpy complexes in acetonitrile [41]. The excitation band observed for these complexes all start from the $^7F_0$ ground term to the $^5D_{0,1,2}$ terms, while emission originates with transitions from the $^5D_0$ excited state to the $^7F_{0,1,2}$ ground levels [41]. The excitation spectrum was collected by monitoring the $^5D_0 \rightarrow {}^7F_2$ emission at 617.25 nm and wide slits were used [41]. In the acetonitrile solution, there is only one $^7F_0 \rightarrow {}^5D_0$ transition located at 17240 cm^{-1} [41]. The $^7F_0 \rightarrow {}^5D_1$ excitation spectrum was collected by monitoring the $^5D_0 \rightarrow {}^7F_2$ emission at 617.7 nm [41]. With excitation at 527.30 nm, a narrow, partially resolved, doublet is observed with a band maxima at 616.35 nm and 617.02 nm [41]. When the complex was excited at the most intense band (527.30 nm) in the $^7F_0 \rightarrow {}^5D_1$, there was no observable

emission in the $^5D_0 \rightarrow {}^7F_0$ region of the spectrum [41]. In contrast, excitation into the weak shoulder at 525.70 nm produces a much broader unresolved emission in the $^5D_0 \rightarrow {}^7F_2$ region and also gives rise to the $^5D_0 \rightarrow {}^7F_0$ emission observed at 580.03 nm [41].

The luminescence behavior of a system containing terpy, Ln^{+3} (Ln = Eu^{+3}, Tb^{+3}, and Gd^{+3}), and poly(*N*,*N*—dimethylacrylamide) (PDMAM) hydrogel has shown to have great photophysical applications [42]. Applications include monitoring phase transformation of the hydrogel itself or of other macromolecules and sensing or monitoring other environment or stimuli [42]. The ligand-lanthanide ion complexes are renown for efficient luminescent agents [42]. They are proficient for emitting a long-lived, narrow band of practically monochromatic radiation by ligand-to-metal energy transfer [42]. They have two major advantages: (1) when excitation is made through the ligand, they solve the problem of small light absorption cross section by lanthanide ions and (2) they protect lanthanide from luminescence quenching processes [42].

In addition to the lanthanides, terpy ligand is also used in the luminescence enhancement of other metals. The ligand emits a very intense luminescence in acidic aqueous solution when excited by 313-nm radiation and is applied as a convenient and sensitive quenching method for the determination of iron [43]. The terpy emission intensity is greater than that of quinine sulfate when both were in the same solution with equal absorbance at the excitation wavelength (313 nm) [43]. Luminescence intensity at 350 nm was measured at different concentrations by varying the pH of the solution [43].

1.6. Tetracyanoplatinates Metal Complex

Another donor system of interest that absorbs in the UV and has been shown to undergo energy transfer processes with select lanthanides cations is the tetracynoplatinates (TCPs) metal complex. Since the observation of the optical properties of TCP in the early 1822, more inclusive studies have been made on the structural and optical properties of the TCP compounds containing a number of diverse cations [33]. The absorption and luminescence properties of many TCP compounds have been studied in detail in a variety of salts with alkali metal, alkaline earth metal, and lanthanide[44] cation, as well as fluid solution [33, 45]. Unlike the alkaline and alkali earth TCPs, the $Ln_2[Pt(CN)_4]_3$-.nH_2O have been reported to exist in two forms: (1) a yellow form (for La^{3+}…….Gd^{3+}) and (2) a red form (for Tb^{3+}…..Yb^{3+}) [44].

The structures of compounds containing TCPs are often characterized by simulated one–dimensional chains of planar anions [18, 33, 46-48]. The significant Pt-Pt interactions that occur between the adjacent TCP anions in these chains, from 3 to 3.7 A, provide highly tunable spectral properties [33, 47]. Experiments have shown that the Pt-Pt distances, and hence the associated spectroscopic properties, can be tuned by chemical and physical variations such as by the choice of countercation or applied pressure [33]. Additionally, in $Ln_2[Pt(CN)_4]_3 \cdot 18H_2O$ (Ln = Sm, Eu) that tetracyanoplatinate excitation can be transferred non-radiatively to the Sm^{3+} or Eu^{3+} ions, respectively, resulting in emission from these cations [33].

The optical properties of crystalline TCP have been studied in detail under variation of temperature, hydrostatic pressure, impurity concentration of $[Ni(CN)_4]^{2-}$ and

$[Pd(CN)_4]^{2-}$ and recently, strong magnetic fields [47]. The magneto-optical investigation show that the crystals emit from three distinct levels, which can be classified within the D_{4h}' symmetry of a single $[Pt(CN)_4]^{2-}$ complex [47]. Examination of the optical properties of tetracyanoplatinates have shown changed considerably, if the compounds are transferred from their dilute aqueous solutions to the crystalline state [45]. This observation is due to a strong coupling between neighboring complex ions in the single crystals, which contain mutually parallel columns of closely stacked $[Pt(CN)_4]^{2-}$ ions [45]. Studies of dilute aqueous solutions of TCP show no emission, for concentrated solutions of TCP containing metals (Ba, Mg, and K), a bright emission has been reported [45].

In the quasi one-dimensional structure, 5d, 6s-HOMO and 6p, CNπ*-LUMO of $[Pt(CN)_4]^{2-}$ overlap and form electronic energy bands [46]. The valence band and conduction band are given by the HUMO and LUMO, respectively [46]. The band widths of TCP depends on the Pt-Pt distances and are several eVs broad (1 eV = 8067 cm^{-1}) [46]. Photoconductivity measurements revealed that the absorption and emission peak energies are not given directly by the band gap energy [46].

Report on the pressure dependence of the photoluminescence spectra of four TCP, M*x*$[Pt(CN)_4]\cdot n H_2O$ (MTCP), with M*x* = KLi, KNa, Cs_2Ca, and Cs_2MTCP's show the crystallize in quasi-one-dimensional (1-D) structures in which the square-planar $[Pt(CN)_4]^{2-}$ units are stacked in columns [48]. The intracolumnar Pt-Pt distance is short compared to the separation from column to column, resulting in a strongly anisotropic interaction between the complex ions, MTCP's show large pressure-dependent shifts of

the optical emission maxima [48]. Three types of spectra were recorded, they include triboluminescence, photoluminescence of small crystals, and photoluminescence of finely ground powders [48]. The relative intensities of the triboluminescence of the samples decrease in the order KNaTCP > KLiTCP > $Cs_2Ca(TCP)_2$ > CsTCP [48]. Hydrostatic high-pressure on the photoluminescence spectra show that all four compounds exhibited a relatively large shift of the emission maximum to lower energies with increasing pressure [48].

The energy level of TCP complex show the ground state in D_{4h} symmetry including spin-orbit coupling to be A'_{1g} arising from the $^1A_{1g}$ state from the (d_z^2) $(d_{xy}, d_{yx})^2$ electron configuration [48]. The first excited state is $^3A_{2u}$ according to the electron transition $5d_z^2 \rightarrow 6p_z, \pi^*(CN)$ [48]. The $^3A_{2u}$ splits into a E'_u and a A'_{1u} when spin-orbit coupling is taken into account [48]. The next higher spin-orbit state is A'_{2u} with $^3E_u/^1A_{2u}$ parentage [48]. The transition between A'_{1g} and the lowest excited state A'_{1u} is symmetry forbidden [48]. However, when electron-phonon coupling with an e_g and a_{2g} vibration is included, relatively weak transitions with $\bar{E} \perp c$ and $\bar{E} \| c$, respectively, are expected [48]. In thermal equilibrium at room temperature practically the whole emission intensity is due to the transition $A'_{1g} \leftarrow A'_{2u}$ $(\bar{E} \| c)$ and $A'_{1g} \leftarrow E'_u$ $(\bar{E} \perp c)$ [48].

1.7. Gold and Silver dicyanides

The structure and spectroscopy of dicyano coordination compounds of Ag(I) and Au(I) have been studied. A temperature-dependent photoluminescence study was carried

out for single crystals of $M[Au(CN)_2]_3$ and $M[Ag(CN)_2]_3$ (M = Tb; Eu; Gd; Y) [49]. The results indicate that in both $Tb[Au(CN)_2]_3$ and $Tb[Ag(CN)_2]_3$, excitation of the donor leads to sensitized luminescence for the acceptor, characteristic of the $^5D_4 \rightarrow {}^7F_J$ (J = 0-6) transition of Tb(III) [49]. The extent of Au-Au and Ag-Ag interaction determined the spectroscopic properties of dicyanoaurate(I) and dicyanoargentate(I) [34, 49].

Application of high pressure at low temperature has been reported to tune the energy transfer process of $Eu[Au(CN)_2]_3$ [34, 49]. The tunability of energy transfer to lanthanide ions is an important aspect for the design of new solid-state systems for technological purposes. Terbium(III) ion is a good candidate as the acceptor in these new materials in which energy transfer is tuned because one of the distinctive feature of Tb(III) is the presence of absorption peaks over a very wide range of energy in the UV and visible regions [49]. Sensitization of the $^5D_4 \rightarrow {}^7F_J$ emission of Tb(III) can occur via energy transfer from strongly absorbing donors that exhibit near-UV or blue-visible luminescence, because of the spectral overlap with the Tb(III) absorption [49]. These ligands are excellent candidates as donor for Tb(III) because their luminescence energies occur over a wide range in the UV and visible regions [49]. Emissions bands that were obtained for Tb(III) include 491 nm ($^5D_4 \rightarrow {}^7F_6$), 543 nm ($^5D_4 \rightarrow {}^7F_5$), 584 nm ($^5D_4 \rightarrow {}^7F_4$), 620 nm ($^5D_4 \rightarrow {}^7F_3$), 647 nm ($^5D_4 \rightarrow {}^7F_2$), 666 nm ($^5D_4 \rightarrow {}^7F_1$) and 677 nm ($^5D_4 \rightarrow {}^7F_0$) [49]. These emissions are based on many spectroscopic studies of the ion in a variety of pure crystals, doped crystals, and solutions. The narrow luminescence bands of the rare-earth ion Tb(III) are due to the $^5D_4 \rightarrow {}^7F_J$ (J = 0-6) transitions [49].

The increased intensity of the excitation profile of the rare earth ion luminescence in the region of the excitation peak of the donor is an indication of energy transfer [49]. Studies have been done on the temperature dependence of the $Tb[Ag(CN)_2]_3$ luminescence using different excitation wavelengths [49]. Dicyanoargentate species are very strong emitters at low temperature. The quenching of this strong luminescence is an illustration of efficient energy transfer from $[Ag(CN)_2^-]$ to Tb(III) in $Tb[Ag(CN)_2]_3$ [49]. The Tb^{3+} acceptor emission is enhanced gradually while the $[Ag(CN)_2^-]$ emission becomes totally quenched as the temperature is increased toward room temperature, in a study that was conducted on the emission of $Tb[Ag(CN)_2]_3$ at 10˚, 100˚, and 270˚ K [49]. An indication that energy transfer is enhanced with temperature increase is illustrated by the temperature dependence for the $Tb[Ag(CN)_2]_3$ emission [49]. The temperature dependence of energy transfer in $Tb[Ag(CN)_2]_3$ can be explained in terms of an exciton model [49]. This shows that excitation energy of the excited donor undergoes significant lattice relaxation before energy transfer takes place. The effectiveness of energy transfer in $Tb[Ag(CN)_2]_3$ is the result of an enhance temperature [49].

Energy transfer from $[Au(CN)_2^-]$ as the donor to Tb^{3+} as the acceptor has also been studied. The similarity between the excitation spectra monitor at the Tb^{3+} and $[Au(CN)_2^-]$ luminescence bands provide evidence for the presence of donor-acceptor energy transfer [49]. Temperature increase leads to an increase of the relative intensities of the higher-energy luminescence bands of $[Au(CN)_2^-]$ [49]. For example, the highest-energy band which is at 395 nm is virtually absent at 10˚ K but becomes the major band at 285˚ K. The luminescence of Tb^{3+} decreases in intensity upon increasing the

temperature [49]. The donor-acceptor spectral over lap increases upon cooling because the [$Au(CN)_2^-$] emission shifts in the direction of a low-energy shoulder [49]. This explains the reason why energy transfer from [$Au(CN)_2^-$] to Tb(III) in $Tb[Au(CN)_2]_3$ is tuned-in by decreasing the temperature [49]. The lifetime decreases with temperature increase from 500 (40) μs to 370 (20) μs with temperature increase from 80˚ K to 170˚ K, respectively [49]. The mechanism of energy transfer in both $Tb[Au(CN)_2]_3$ and $Tb[Ag(CN)_2]_3$ is the Dexter exchange mechanism [49]. This mechanism occurred in systems that have a short donor-acceptor separation and the occurrence of a bimolecular collision between the donor and acceptor [49]. As a result, the Dexter mechanism is dominant when the donor-acceptor distance is short and when significant overlap exists between the molecular orbitals of the two species [49].

The photoluminescence spectra of [EuAu] and [EuAg] have been studied and compared. When the intensity of the region covering the Eu^{3+} ion $^5D_0 \rightarrow {}^7F_0$ transitions were recorded at 78 K, six well-resolved bands are observed [34]. The energies on these lines along with their assignments are given in Table (1.1 & 1.2). The emission spectrum of [EuAg] recorded at 10 K only showed four peaks observable over the Eu^{3+} ion $^5D_0 \rightarrow {}^7F_0$, $^7F_1$ transition regions.

Temperature-dependent photoluminescence spectra of [EuAu] consist of sharp emission lines that are characteristic of Eu^{3+} f-f transitions [34]. There is a significant decrease in the emission intensity of Eu^{3+} as the temperature increase [34]. Compare to the emission intensity of [EuAu], the intensity of [EuAg] increases when temperature is increased [34].

Table 1.1. Assignments of Bands for the High-Resolution Eu^{3+} Emission Spectrum of the [EuAu] complex [41].

Emission band λ, nm	Emission Energy , cm^{-1}	Rel. intensity	Assignment
584.1	17120	0.18	$^5D_0 \rightarrow {}^7F_0$
585.1	17090	0.13	$^5D_0 \rightarrow {}^7F_0$
589.2	16970	0.54	$^5D_0 \rightarrow {}^7F_1$
590.2	16930	0.24	$^5D_0 \rightarrow {}^7F_1$
592.0	16890	0.62	$^5D_0 \rightarrow {}^7F_1$
593.1	16860	1.00	$^5D_0 \rightarrow {}^7F_1$

Both the $Au(CN)_2^-$ and $Ag(CN)_2^-$ emissions are completely quenched by Eu^{3+} ion, there by indicating an efficient energy-transfer process in the complexes [34]. The low emission intensity of the [EuAu] complex suggests that at higher temperatures a nonradiative deexcitation process via a charge-transfer state competes with the radiative pathway [34]. The emission intensity of the Eu^{3+} ion decreases with an increase in temperature because increase in temperature pushes the donor level to an higher position and the overlap with the $^5D_3$ acceptor state diminishes [34]. As a result, the charge transfer state increasingly dominate in accepting the energy [34].

Table 1.2. Assignments of Bands for the High-Resolution Eu^{3+} Emission Spectrum of the [EuAg] complex [41].

Emission band λ, nm	Emission Energy , cm^{-1}	Assignment
558.1	17917	$^5D_1 \rightarrow {}^7F_1$
581.0	17210	$^5D_0 \rightarrow {}^7F_0$
586.2	17050	$^5D_0 \rightarrow {}^7F_1$
590.5	16935	$^5D_0 \rightarrow {}^7F_1$
594.5	16820	$^5D_0 \rightarrow {}^7F_1$
614.2	16280	$^5D_0 \rightarrow {}^7F_2$
616.6	16220	$^5D_0 \rightarrow {}^7F_2$
619.8	16130	$^5D_0 \rightarrow {}^7F_2$
626.1	15970	$^5D_0 \rightarrow {}^7F_2$
628.4	15910	$^5D_0 \rightarrow {}^7F_2$

CHAPTER 2

EXPERIMENTAL METHODS

2.1. Materials and Methods

All synthetic work along with IR and Single-Crystal X-ray Diffraction were conducted at the University of South Alabama. The following chemicals were used for the syntheses as received without further purification. $Eu(NO_3)_3 \cdot 6H_2O$ (Alfa Aesar, 99.9%), $Eu(CF_3SO_3)_3 \cdot x$H2O (Alfa Aesar, 98%), $Eu(CH_3\text{-}COO)_3 \cdot xH_2O$ (Alfa Aesar, 99.9%), 2,2**:**6 ,2-terpyridine (Alfa Aesar, 97%), and $K_2Pt(CN)_4 \cdot 3H_2O$ (Alfa Aesar, 99.9%). The reaction conditions given below produced the highest yields of the respective compounds. The Jasco FT/IR-4100 with a diamond ATR setup was utilized to obtained IR spectra at room temperature.

2.2. Synthesis

2.2.1. Synthesis of $Eu(C_{15}H_{11}N_3)(H_2O)_2(NO_3)(Pt(CN)_4)_3CH_3CN$ (1)

The synthesis of **1** was carried out by first mixing 1 mL of 0.12 M $Eu(NO_3)_3$ and **1** mL of 0.15 M $K_2[Pt(CN)_4] \cdot 3H_2O$. Next 1 mL solution of 0.10 M terpy was layered onto the mixture. The $Eu(NO_3)_3$ and terpy solutions were prepared using CH_3CN as the solvent, while the $K_2[Pt(CN)_4] \cdot 3H_2O$ in a 1:4 mixture of water/CH_3CN. Evaporation of the solvent over a period of 2 weeks resulted in the crystallization of **1** as colorless single crystals with a yield of 57.6%. IR(solid, cm^{-1}): 3244 (s, br), 2193 (w), 2166 (w), 2148 (s),

1600 (m), 1580 (m), 1482 (s), 1451 (s), 1422 (m, sh), 1304 (s), 1234 (m), 1196 (w), 1158 (m), 1075 (w), 1038 (m), 1015 (s), 813 (m), 786 (s).

2.2.2. Synthesis of {Eu($C_{15}H_{11}CN_3$)(H_2O)$_3$}$_2$(Pt(CN)$_4$)$_3$•2H_2O (2)

The synthesis of **2** was carried out by first mixing 1 mL of 0.10 M Eu(CF_3SO_3)$_3$ and 1 mL of 0.15 M K_2[Pt(CN)$_4$]. Next 1 mL of a 0.10 M 2,2′:6′,2″-terpyridine solution was layered on top. The terpyridine solution was prepared using CH_3CN as the solvent, while the Eu(CF_3SO_3)$_3$ and K_2[Pt(CN)$_4$] solution were prepared in 1:4 solutions of water/ CH_3CN. Evaporation of the solvent over a period of a week resulted in the crystallization of **2** as colorless single crystals with a yield of 44.4%. IR(solid, cm^{-1}): 3361 (s, br), 3100 (w, br), 2181 (w), 2160 (w, sh), 1450 (m), 1435 (s), 1399 (w), 1312 (m), 1268 (m), 1236 (m), 1196 (m), 1173 (w, sh), 1162 (s), 1078 (w), 1032 (m), 1013 (s), 904 (w), 771 (s), 742 (m), 669 (m).

2.2.3. Synthesis of {Eu($C_{15}H_{11}CN_3$)(H_2O)$_2$(CH_3COO)$_2$]$_2$Pt(CN)$_4$•3H_2O (3)

The synthesis of **3** was carried out by first mixing 1 mL of 0.10 M aqueous Eu(CH_3COO)$_3$ and 1 mL of 0.025 M K_2[Pt(CN)$_4$]. Next, a 1 mL solution was prepared using CH_3CN as the solvent, while the K_2[Pt(CN)$_4$] solution was made by dissolving the K_2[Pt(CN)$_4$] · 3H_2O in a 1:4 mixture of water/ CH_3CN. Slow evaporation of the solvent over a period of several days resulted in the crystallization of 3 as colorless single crystals with a yield of 63.9%.n IR(solid, cm^{-1}): 3628 (m), 3550 (w, br), 3407(w, br), 2134 (s), 2122 (s), 1616 (s), 1559 (m), 1455 (w), 1422 (m), 761 (m), 669 (m), 656 (m).

2.3. Single-Crystal X-ray Diffraction

Single crystals of **1-3** with dimensions of 0.476 mm x 0.268 mm x 0.078 mm, 0.460 mm x 0.166 mm x 0.120 mm, and 0.900 mm x 0.244 mm x 0.232 mm, respectively, were selected, mounted on quartz fibers, and aligned on an Enraf-Nonius CAD-4 single-crystal X-ray diffractometer with an optical microscope. Intensity measurements were performed using graphic monochromated Mo Kα radiation from a sealed tube. Three standard collections were collected every 2 h to monitor for crystal decay. The intensities of the reflections were collected using θ/2θ scans.

All of the crystals examined in the studies diffracted extremely well and were non-problematic in regards to data collection and structure analysis. XCAD4 was used to process the raw X-ray data. The program suite SHELXTL (v 5.1) was used for space group determination and application of absorption corrections (XPREP), structure solution (XS), and least squares refinement (XL). The initial structure solutions were carried out using direct methods, and the remaining atomic positions were located in difference maps. For **1** and **3**, analytical absorption corrections were applied to the data, while a psi-scan absorption correction was applied for **2**. The final refinements included anisotropic displacement parameters for all non hydrogen atoms.

2.4. Photoluminescence Measurements

The luminescence spectra were collected using a photon technology international (PTI) spectrometer (model QM-7/SE). The system uses a high intensity xenon source for excitation. Selection of excitation and emission wavelengths are conducted by means of

computer controlled autocalibrated “QuadraScopic” monochromators and are equipped with aberration corrected emission and excitation optics. Signal detection is accomplished with a PMT detector (model 928 tube) that can work either in analog or digital (photon counting) modes. All of the emission spectra presented are corrected to compensate for wavelength dependent variation in the system on the emission channel. The emission correction files which were generated by comparison of the emission channel response to the spectrum of NIST traceable tungsten light were used as received from Photon Technology International (PTI). The emission correction was conducted in real time using the PTI provided protocol. The instrument operation, data collection, and handling were all controlled using the advanced FeliX32 fluorescence spectroscopic package. The steady state emission and excitation spectra were collected upon continuous excitation (without introducing any time delay). All of the spectroscopic experiments were conducted on neat crystalline samples held in sealed quartz capillary tubes. The low temperature measurements were conducted on samples inserted in a coldfinger Dewar flask filled with liquid nitrogen.

The samples were studied at both liquid nitrogen and room temperature. Comparison of both temperatures were accomplished by conducting the experiment at liquid nitrogen in the coldfinger Dewar and the sample was kept overnight while maintaining the same parameters. The room temperature data was collected after the evaporation of liquid nitrogen overnight. Excitation and emission are the two spectra that are normally taken during luminescence measurement. To obtain excitation, emission is

held at a constant value while running the excitation and for emission the excitation is held constant.

CHAPTER 3

RESULTS AND DISCUSSIONS

3.1. Photoluminescence Studies of $Eu(C_{15}H_{11}N_3)(H_2O)_2(NO_3)(Pt(CN)_4)_3CH_3CN$ (1)

The structure of **1** (Figure 3.1) show that the coordination of the Eu site is 9-fold and can be described as distorted [EuO_4N_5] tricapped trigonal prism. There are five nitrogen atoms in the inner sphere of the Eu^{3+} that originate from one tridentate terpyridine ligand and two N-bound $Pt(CN)_4^{2-}$ anions. Additionally, there are four oxygen atoms that are coordinated to the Eu^{3+} that originate from one bidentate nitrate anion and two coordinated water molecules. As a result of the coordination between the donor anions (TCP and terpy) and the acceptor cation (Eu^{3+}) there is transfer of energy from the donor to the acceptor.

The photoluminescence (PL) spectra of **1** are shown in Figure 3.2. The excitation spectrum (a) shown in Figure 3.2 was monitored at the Eu^{3+} emission at 614 nm. The spectrum consists of a broadband maximizing at ~360 nm in addition to the overlaying sharp f-f transitions corresponding to f-f excitation of the Eu^{3+} ion. This broadband is uncommon of f-f transitions and it suggests a donor/acceptor type interaction. Only the europium emission (Figure 3.2b) is observed upon excitation of the donor system at 393 nm. Confirmation of the existence of intermolecular energy transfer (IET) in **1** shown by the observance of a broad excitation band while monitoring the europium emission.

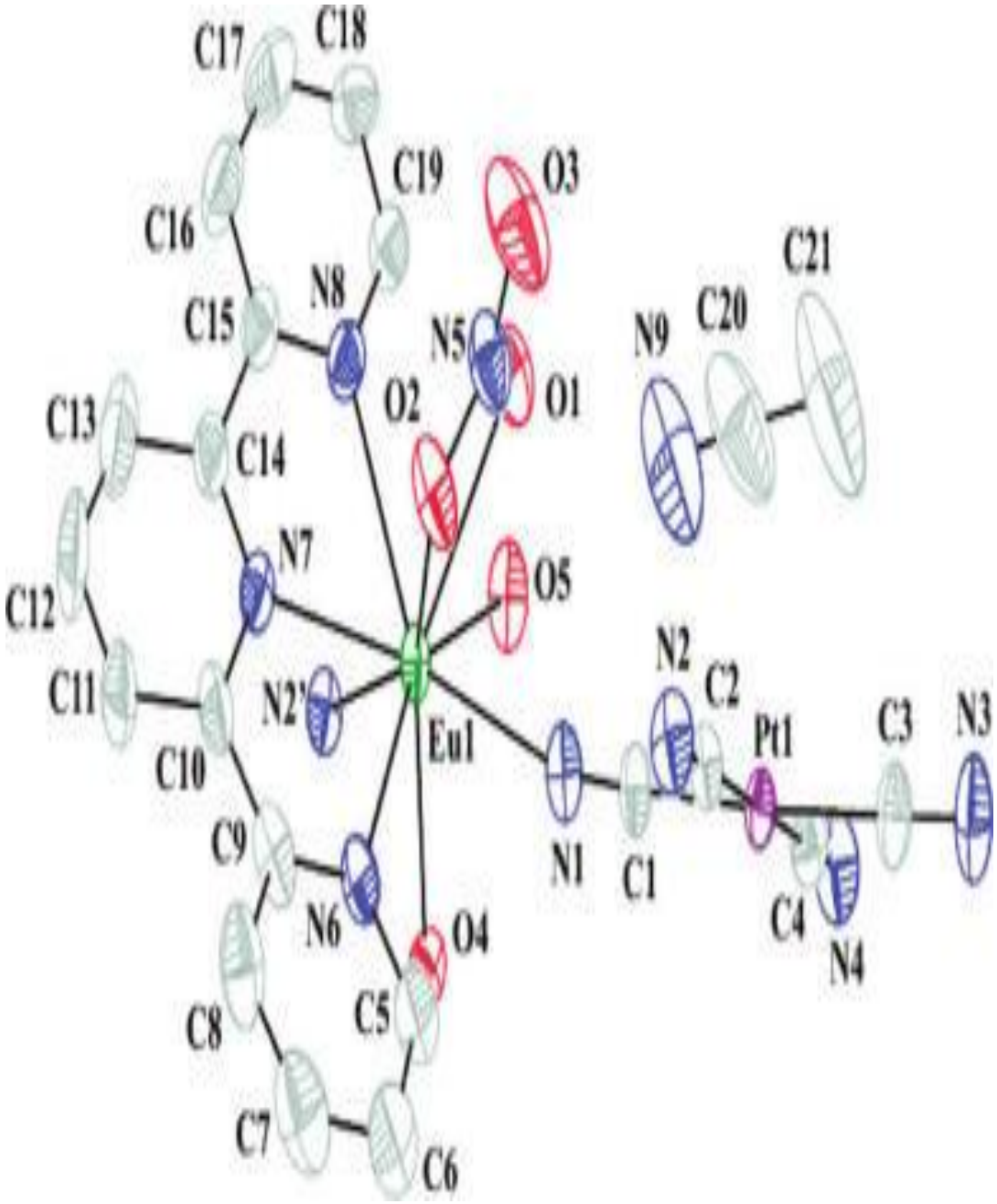

Figure 3.1. Structure of 1 illustrating the coordination environment of the Eu^{3+} ion.

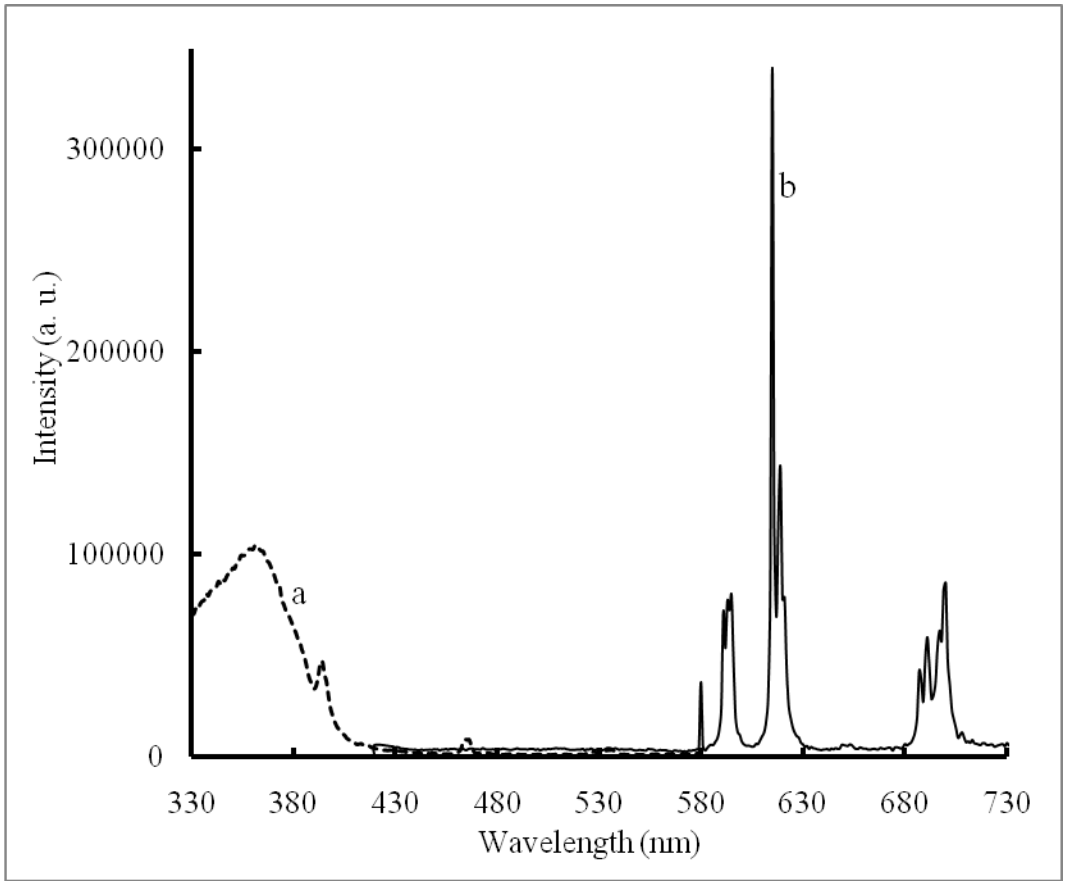

Figure 3.2. Photoluminescence spectra of 1: (a) Excitation spectrum monitored at the Eu^{3+} emission line at 614 nm; (b) Emission spectrum with excitation wavelength at 395 nm.

Our studies indicate that both tetracyanoplatinate and the terpyridine ligand act as sensitizers of the Eu^{3+} cation. As a result, an efficient intermolecular energy transfer (IET) process exists in this system. Additionally, the total absence of emission assignable to the $Pt(CN)_4^{2-}$ group and the dominance sharp emissions characteristic of f-f transitions within the Eu^{3+} ion are evidence of IET in **1**. When compared with the room temperature data the emission intensities are enhanced significantly at liquid N_2 temperature. The

appearance of a broad excitation band upon monitoring at the Eu^{3+} emission is a direct evidence for donor/acceptor type energy transfer. Conclusion that both the terpyridine ligand and the metal-centered triplet state of $Pt(CN)_4^{2-}$ operate as sensitizers of the Eu^{3+} emission is shown by the excitation profile [33].

3.2. Photoluminescence Studies of $\{Eu(C_{15}H_{11}CN_3)(H_2O)_3\}_2(Pt(CN)_4)_3 \bullet 2H_2O$ (2)

Compared to **1**, the Eu^{3+} in **2** has a coordination number of nine. The structure of **2** contains Eu^{3+} cations linked by both cis- and trans-bridging tetracyanoplatinate anions as shown in Figure 3.3. The coordination sphere of the one Eu^{3+} site in the structure of **2**, contains one tridentate terpyridine ligand, three coordinated water molecules, and three N-bound cyano groups from the bridging tetracyanoplatinate moieties. The geometry of **2** is nearly a regular tricapped trigonal prism. The coordination of two $Pt(CN)_4^{2-}$ groups to the acceptor (Eu^{3+}) cation lead to more energy being transfer to Eu^{3+}, as a result the luminescence features of **2** are more enhance compared to **1**.

A similar spectral profile is observed for **2** (Figure 3.4), where the nitrate counter anion is replaced by a non-coordinating *triflate* anion. When the excitation spectrum was collected by monitoring the Eu^{3+} emission at 617 nm the spectrum consists of a broad band that maximizes at ~355 nm at both room and liquid N_2 temperatures. Furthermore, there is a shoulder at 375 nm. In addition, the characteristic f-f transitions corresponding to the Eu^{3+} ion are also observed.

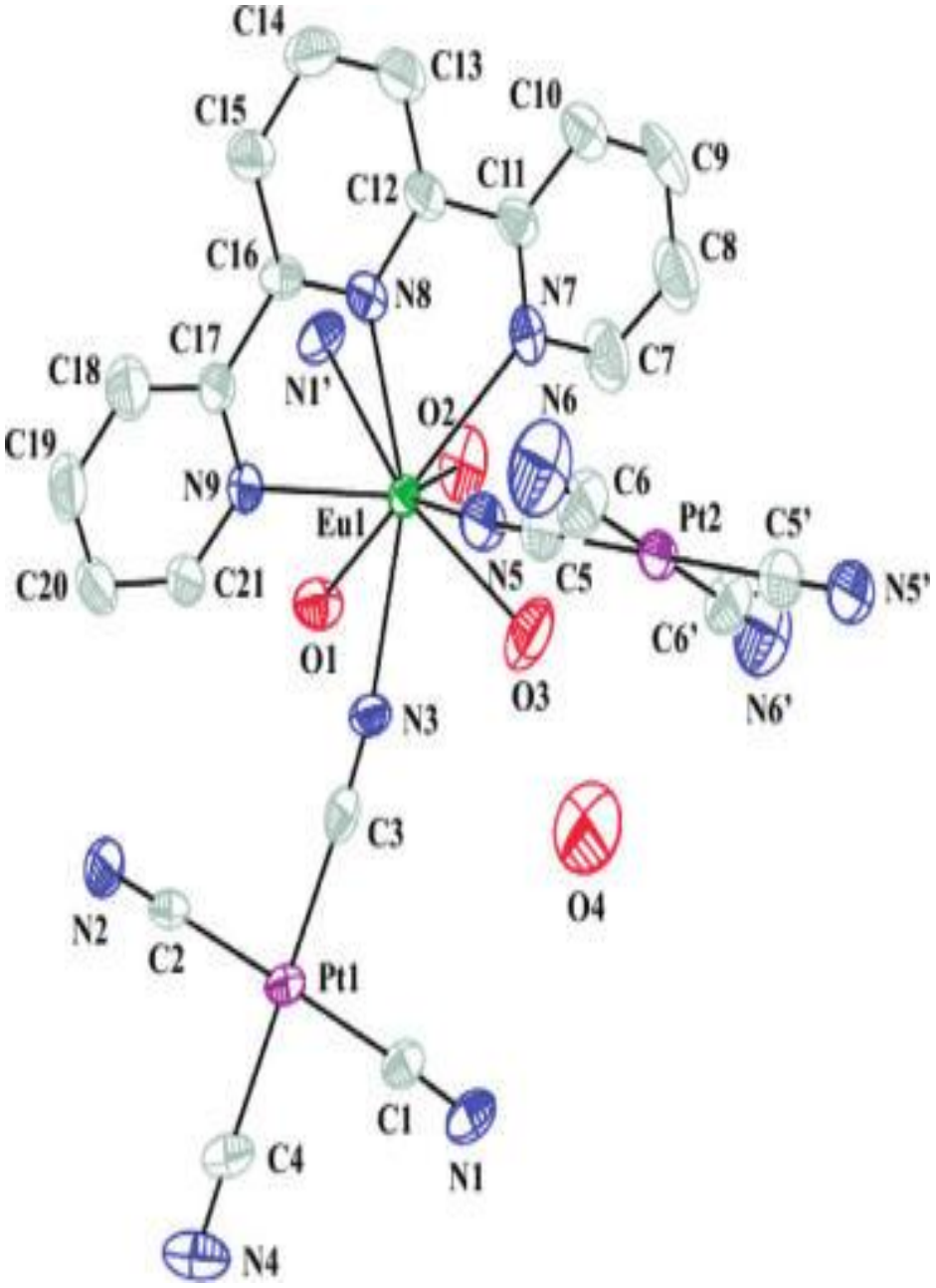

Figure 3.3. Structure of 2 illustrating the coordination environment of the Eu^{3+} ion.

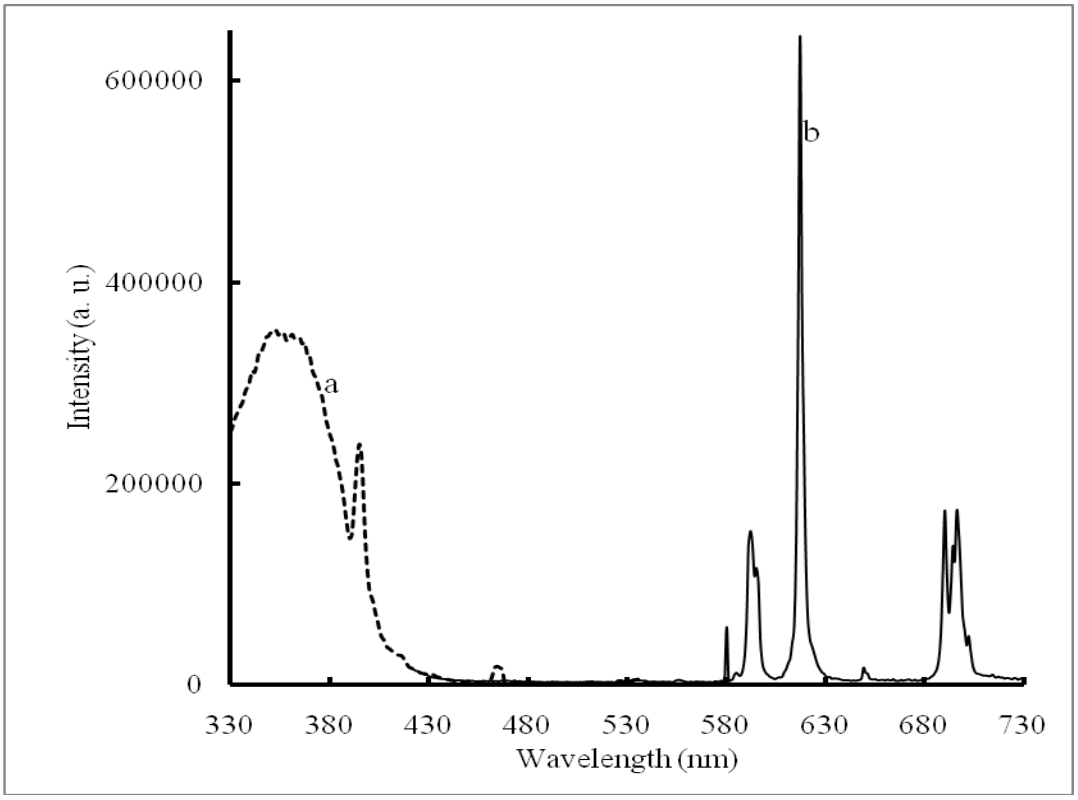

Figure 3.4. Excitation (a) and Emission (b) of 2 excited at 395nm and monitored at 617 nm, respectively.

The emission spectrum of **2** shown in Figure 3.4b was collected upon excitation at 395 nm. The wavelength corresponds to direct f-f $^5L_6 \leftarrow {}^7F_0$ transition. Evidence of f-f transition is provided by a series of sharp bands in the 580–702 nm range that originate from the $^5D_0$ excited state. The single peak at 580 nm is a result of the $^5D_0 \rightarrow {}^7F_0$ transition and it corresponds to a single Eu^{3+} site in the lattice. At 591 and 595 nm is the $^5D_0 \rightarrow {}^7F_1$ and these peaks are separated by 110 cm^{-1}. The most intense peak is at 617 nm which correspond to the $^5D_0 \rightarrow {}^7F_2$ transition. The existence of more than one emitting state in the scheme is shown in the emission profile by the weak but sharp elevated

energy bands at 536 nm and 556 nm. Both of these bands start from the second highest excited state of Eu^{3+} and correspond to the $^5D_1 \rightarrow {}^7F_1$ and $^7F_2$ transitions [33].

The occurrence of sharp bands in the spectrum is a significant feature of Eu^{3+} ion f-f transitions. Detail assignments of these transitions are shown in Table 3.1. In the low temperature spectrum there is a band originating from the higher $^7F_1$ level [33]. As a result of this band, there is evidence of the $^5D_1 \leftarrow {}^7F_1$ transition. The lacking of this band in the low temperature spectrum suggests that thermal population from the ground $^7F_0$ to the $^7F_1$ state is important in inducing the optical transition.

Table 3.1. Excitation and Emission Data for 2

Excitation bands nm	Excitation bands cm^{1-}	Assignment	Emission bands nm	Emission bands cm^{1-}	Assignment
355	28200	$\pi - \pi^*$ (terpy)	454	22020	$^5D_2 \rightarrow {}^7F_1$
375	26700	CT $(Pt(CN)_4^2$	527	18980	$^5D_1 \rightarrow {}^7F_0$
395	25300	$^5L_6 \leftarrow {}^7F_0$	536	18660	$^5D_1 \rightarrow {}^7F_1$
415	24100	$^5D_3 \leftarrow {}^7F_0$	556	17990	$^5D_1 \rightarrow {}^7F_2$
465	21500	$^5D_2 \leftarrow {}^7F_0$	580	17250	$^5D_0 \rightarrow {}^7F_0$
525	19050	$^5D_1 \leftarrow {}^7F_1$	591	16900	$^5D_0 \rightarrow {}^7F_1$
534	18700	$^5D_1 \leftarrow {}^7F_1{}^*$	595	16790	$^5D_0 \rightarrow {}^7F_1$
			617	16200	$^5D_0 \rightarrow {}^7F_2$
			649	15400	$^5D_0 \rightarrow {}^7F_3$

*This band is not present in the low temperature spectrum [33]

Figure 3.5 shows the excitation spectra of **2**, monitored at the Eu^{3+} emission line at 617 nm. These peaks dominate in both liquid N_2 and room temperature. Figure 3.5a shows the excitation spectra of **2** at liquid N_2 and room temperature (3.5b). Both spectra contain a dominate broad excitation band which is centered at ~350 – 355 nm, albeit shaper at the liquid N_2 temperature (Figure 3.5a). Additionally, both spectra contain a shoulder at 375 nm that is well resolved at the liquid N_2 spectrum. These excitation bands are not characteristic of f-f transitions although the emission bands of Eu^{3+} ion were observed upon excitation with the 350 nm wavelength. Hence it is obvious that the phenomenon is characteristic of sensitized emission from **2** achieved through $Pt(CN)_4^{2-}$ antenna triplet states and/or a terpyridine $\pi - \pi^*$ intraligand transition.

There is an overlap in the 300–400 nm region of the excitation spectra of the two sensitizers (terpy and tetracyanoplatinate), where the direct coordination of both the terpy ligand and the $Pt(CN)_4^{2-}$ ensure the sensitization of **2** as indicated by the broad excitation band covering the near UV region. There is no emission originating from the $Pt(CN)_4^{2-}$ anion in the visible region for **1** and **2**, at both temperatures. This is consistent with the argument presented in the introduction where energy transfer to the acceptor Eu^{3+} ion proceeds efficiently quenching donor $Pt(CN)_4^{2-}$ emission entirely. The evidence of energy transfer in the system is demonstrated when the acceptor Eu^{3+} is monitored and the donor groups reveal strong excitation bands.

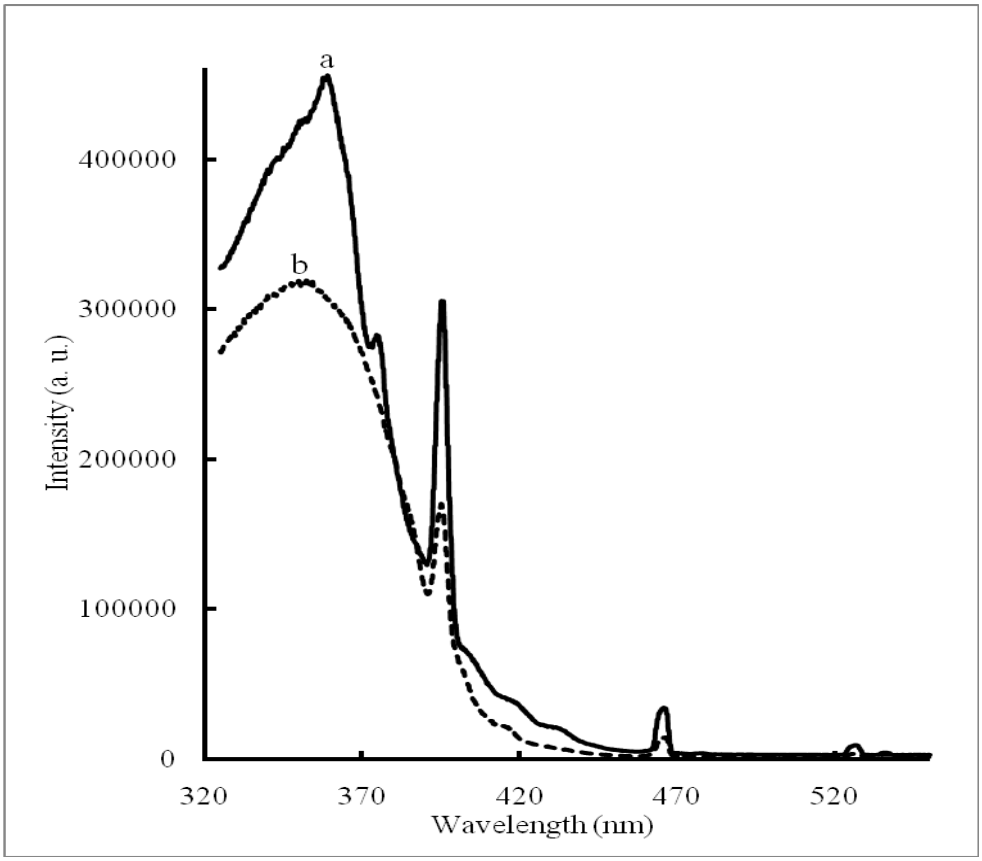

Figure 3.5. Excitation spectra of 2 collected at liquid N_2 (a) and room temperature (b). Both spectra were collected by monitoring the Eu(III) emission at 617 nm.

3.3. Photoluminescence Studies of $[Eu(C_{15}H_{11}CN_3)(H_2O)_2(CH_3COO)_2]_2Pt(CN)_4 \cdot 3H_2O$ (3)

In contrast to the structures of **1** and **2** described above, the $Pt(CN)_4^{2-}$ does not coordinate to the Eu^{3+} cation in **3** as shown in Figure 3.6. Furthermore, there are also the presences of three uncoordinated waters of hydration found in the structure. The coordination environment of the Eu^{3+} ion consist of one tridentate terpy ligand,

two bidentate acetate anions, and two water molecules which provide a total of nine inner sphere coordination around the metal center. The lack of coordination between the donor $Pt(CN)_4^{2-}$ and the acceptor Eu^{3+} has implications on the potential for energy transfer between them as described in the spectroscopic data.

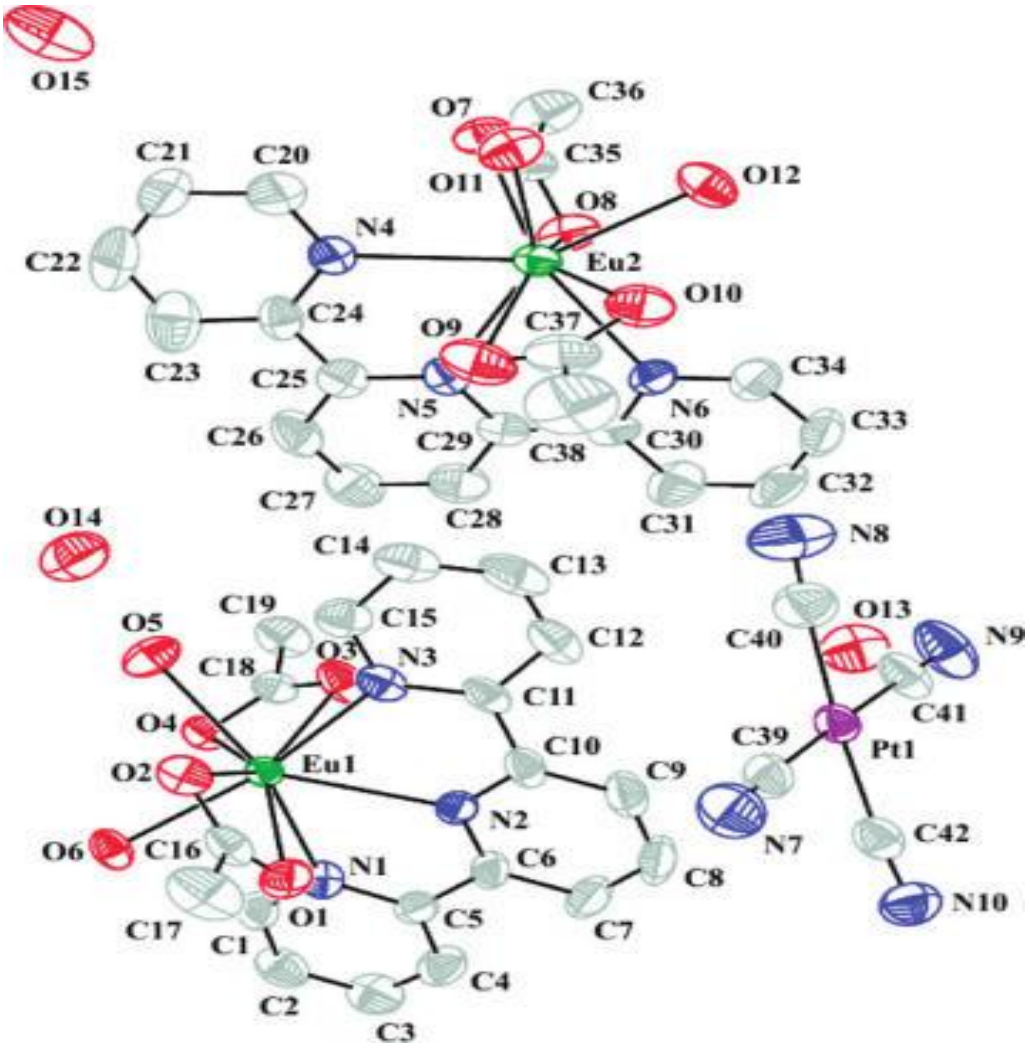

Figure 3.6. Structure of 3 illustrating the coordination environment of the Eu^{3+} ion.

The photoluminescence spectra shown in Figure 3.7 illustrate significant changes in the emission profiles when the excitation wavelength changes from 350 nm to longer wavelengths. This is because of the changes in the structural features of **3** which lack the direct bonding between the Eu^{3+} ion and the $Pt(CN)_4^{2-}$ group. The donor/acceptor energy transfer process in **3** is altered as a result of the structural change when compared with **1** and **2**. At 350 nm excitation, a weak broad emission emerges at 502 nm, and its intensity increases systematically with an increase in the excitation wavelength, achieving a maximum intensity at ~390 nm excitation. When the wavelength increases beyond 390 nm, the intensity of the broadband emission is reduced with a concomitant decrease in the intensities of the sharper f-f emissions. These changes are compared in Figures 3.8 where the dependence of the ratios of the emission intensities are compared as function of the excitation wavelength.

In Figure 3.9 are shown the excitation spectra of compound **3** monitored at the Eu^{3+} emission line at 617 nm (Figure 3.9a) and at the $Pt(CN)_4^{2-}$ emission band 502 nm (Figure 3.9b). The spectrum shown in Figure 3.9a was collected by monitoring the Eu^{3+} ion emission at 617 nm, and consists of a broadband centered at ~350 nm that falls off sharply at the longer wavelength side, and has a shoulder on the shorter wavelength side. Figure (3.9b) corresponds to the excitation spectrum monitored at the broad (502 nm) emission band. An entirely different excitation profile is observed, where a broadband that maximizes at ~390 nm dominates the spectrum. There is also a dip found in the broad excitation band at ~395 nm (Figure 3.9b). The dotted line in the figure is drawn to emphasize the correlation of the spectral dip at the 395 nm excitation band. Figure 3.8

represents the dependence of the ratios of the emission intensities on excitation wavelength.

Observation from Figures 3.7 and 3.8 illustrate that the intensity ratio of the Eu^{3+} emission peak height vs the broadband emission (616:502 nm) decreases significantly as the excitation wavelength changes from 350 nm to a longer wavelength. At 350 nm the ratio is 111 and reduced to 17 at 360 nm. The intensity ratio continuously drops as the excitation wavelength increases further. The ratio at 370, 380, 390, and 400 nm are 3.2, 1.0, 0.5, and 0.7, respectively. There is an increase in the intensity at 400 nm (0.7) which is the result of direct excitation of Eu^{3+} into the $^5L_6$ transition state.

The dotted line in Figure 3.9 represent the correlation of the spectral dip with the 395 nm excitation band. Occurrence of the dip signifies that part of the excitation energy at 395 nm is absorbed by the Eu^{3+} ion, plummeting the intensity of the emission from the $Pt(CN)_4^{2-}$ group. Therefore, the emission intensity of **3** drops when excited at 395 nm giving a slight increase in the intensity ratio as stated early. This phenomenon leads to the observation of efficient non-radiative energy transfer between the Eu^{3+} and $Pt(CN)_4^{2-}$ [33].

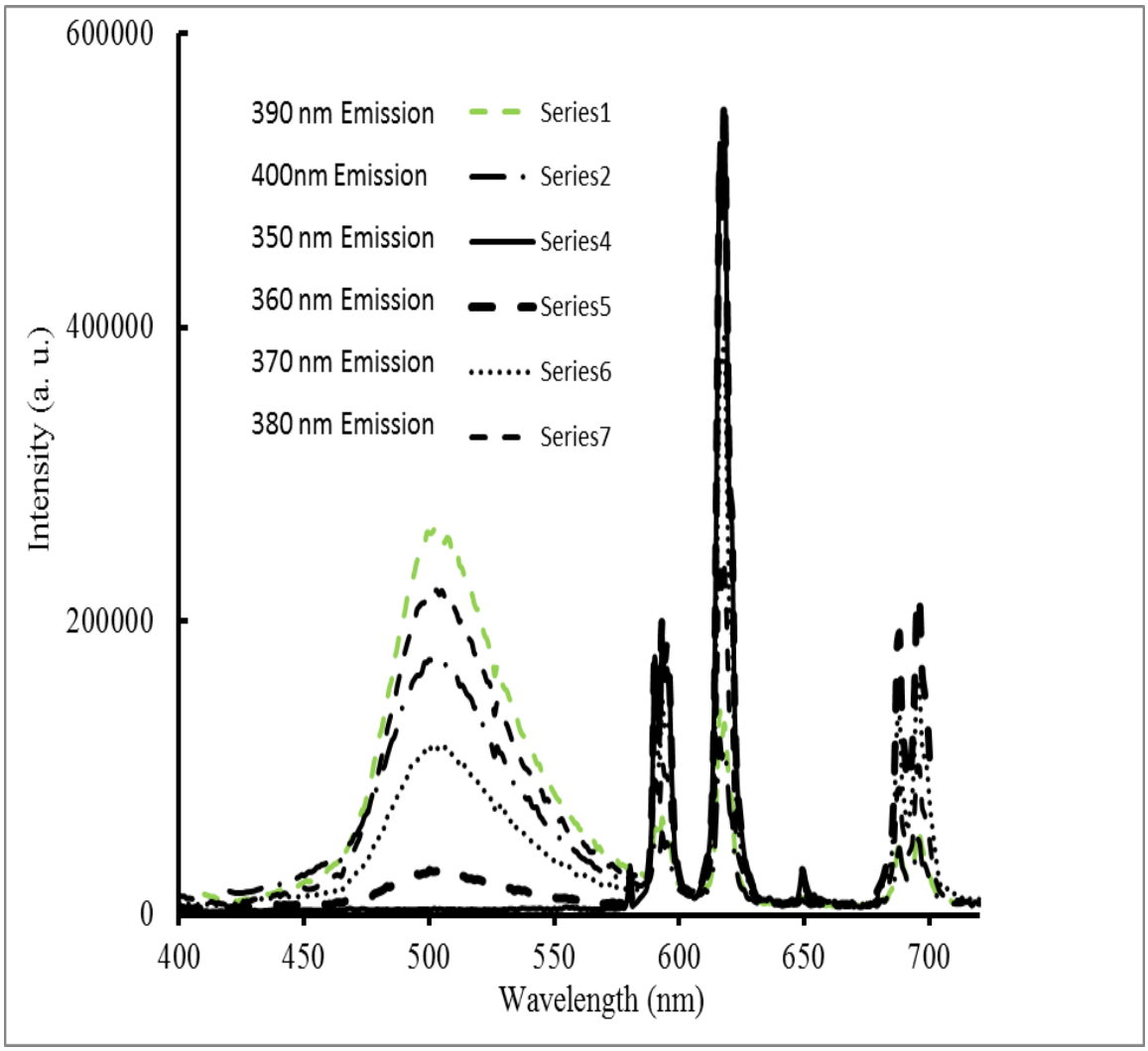

Figure 3.7. Emission spectra of 3 resulting from excitation at 350 nm, 360 nm, 370 nm, 380 nm, 390 nm, and 400 nm. All spectra were collected at room temperature.

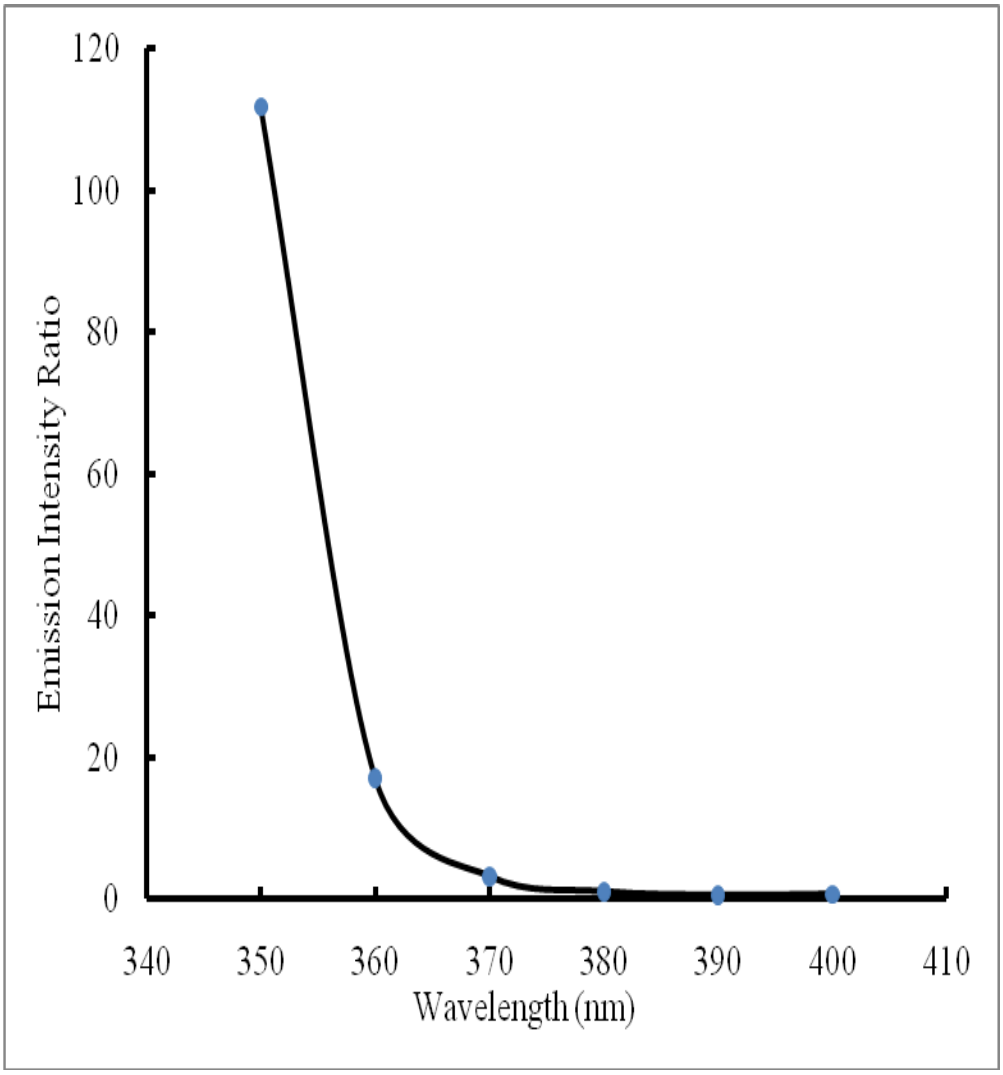

Figure 3.8. Dependence of the emission intensity ratio (616:502 nm) on excitation wavelength for 3.

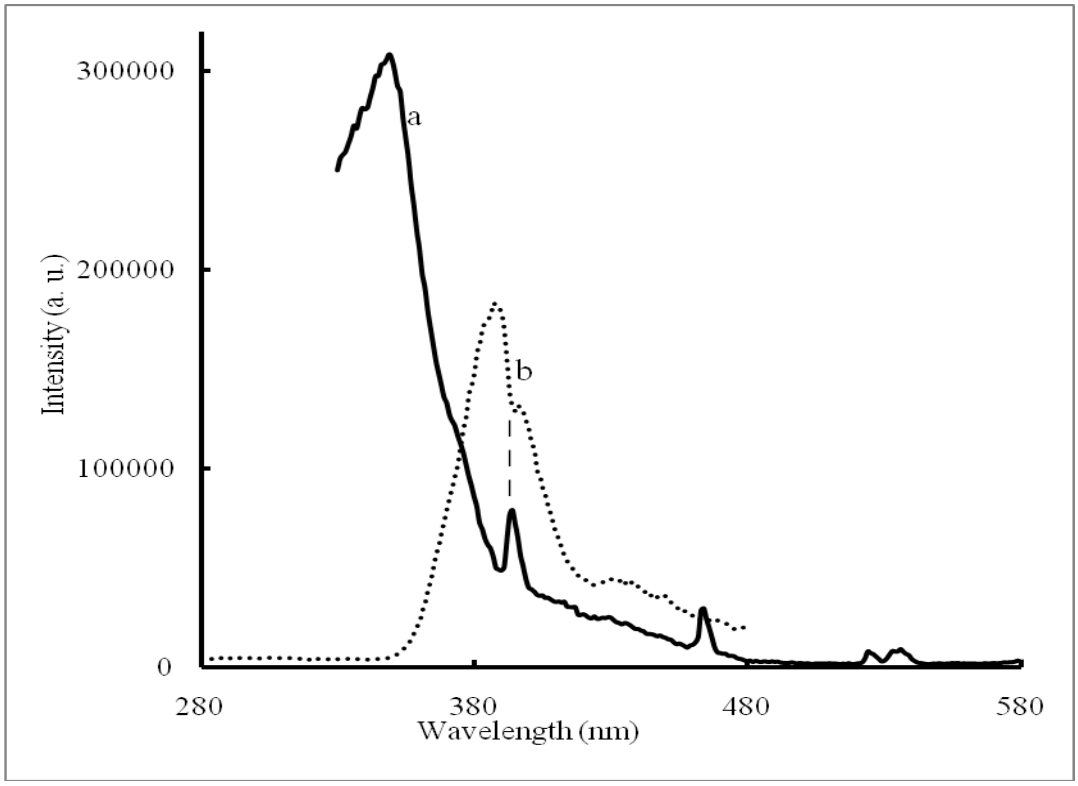

Figure 3.9. Excitation spectra of 3: (a) monitored at the Eu(III) emission line at 617 nm; (b) monitored at tetracyanoplatinate emission at 502 nm. Note the correlation between the dip in spectrum b and the 395 nm excitation band in spectrum a. The dotted line is drawn to guide the eye to this correlation.

There is the existence of a strong excited state energy transfer between the terpy ligand and the Eu^{3+} ion because of the observance of the Eu^{3+} emission upon excitation at wavelength shorter than 350 nm. The effectiveness of energy transfer decreases proportionately because of the sharp drop of the excitation band when **3** is excited at wavelength greater than 340 nm, therefore the Eu^{3+} emission decreases as the excitation wavelength progresses to longer wavelength [33]. Detail assignments of the Eu^{3+}

transitions are shown in Table 3.2. In contrast, as the excitation wavelength approaches a maximum value of 390 nm the $Pt(CN)_4^{2-}$ emission increases in intensity. Nevertheless, there is a decrease in the $Pt(CN)_4^{2-}$ and increase in Eu^{3+} emission at ~395 nm, this is expected because Eu^{3+} absorbs at this wavelength [33]. As a result of the observations from the spectra of **3**, only the terpyridine group efficiently transfers its excited energy non-radiatively to the Eu^{3+} ion in **3,** and a radiative mechanism is evident from the $Pt(CN)_4^{2-}$ group.

Table 3.2. Excitation and Emission Data for 3.

Excitation bands (nm)	Excitation bands (cm^{1-})	assignment	Emission bands (nm)	Emission bands (cm^{1-})	assignment
350	28570	$\pi - \pi^*$ (terpy)	503	19870	$Pt(CN)_4^{2-}$
390	25640	CT ($Pt(CN)_4^{2-}$	580	17240	$^5D_0 \rightarrow {}^7F_0$
395	25320	$^5L_6 \leftarrow {}^7F_0$	590	16950	$^5D_0 \rightarrow {}^7F_1$
465	21500	$^5D_3 \leftarrow {}^7F_0$	593	16860	$^5D_0 \rightarrow {}^7F_1$
526	19010	$^5D_2 \leftarrow {}^7F_0$	595	16810	$^5D_0 \rightarrow {}^7F_1$
535	19690	$^5D_1 \leftarrow {}^7F_1$	616	16230	$^5D_0 \rightarrow {}^7F_2$
538	18590	$^5D_1 \leftarrow {}^7F_1$	618	16180	$^5D_0 \rightarrow {}^7F_2$
			649	15400	$^5D_0 \rightarrow {}^7F_3$
			688	14530	$^5D_0 \rightarrow {}^7F_4$
			695	14390	$^5D_0 \rightarrow {}^7F_4$

*****This band is not present in the low temperature spectrum [33]

3.4. Photoluminescence Studies of $Tb(C_{15}H_{11}N_3)(H_2O)(NO_3)_2(Au(CN)_2)$ (4)

Figure 3.10 and 3.11 show the emission and excitation spectra of compound **4** at liquid N_2, respectively. The emission spectra show peaks at 488, 542, 582, 620, 643, 663, and 673 nm. The 542 nm peak is the most intense. Excitation spectra show peaks at 352 nm, 363 nm, 378 nm, and 487 nm.

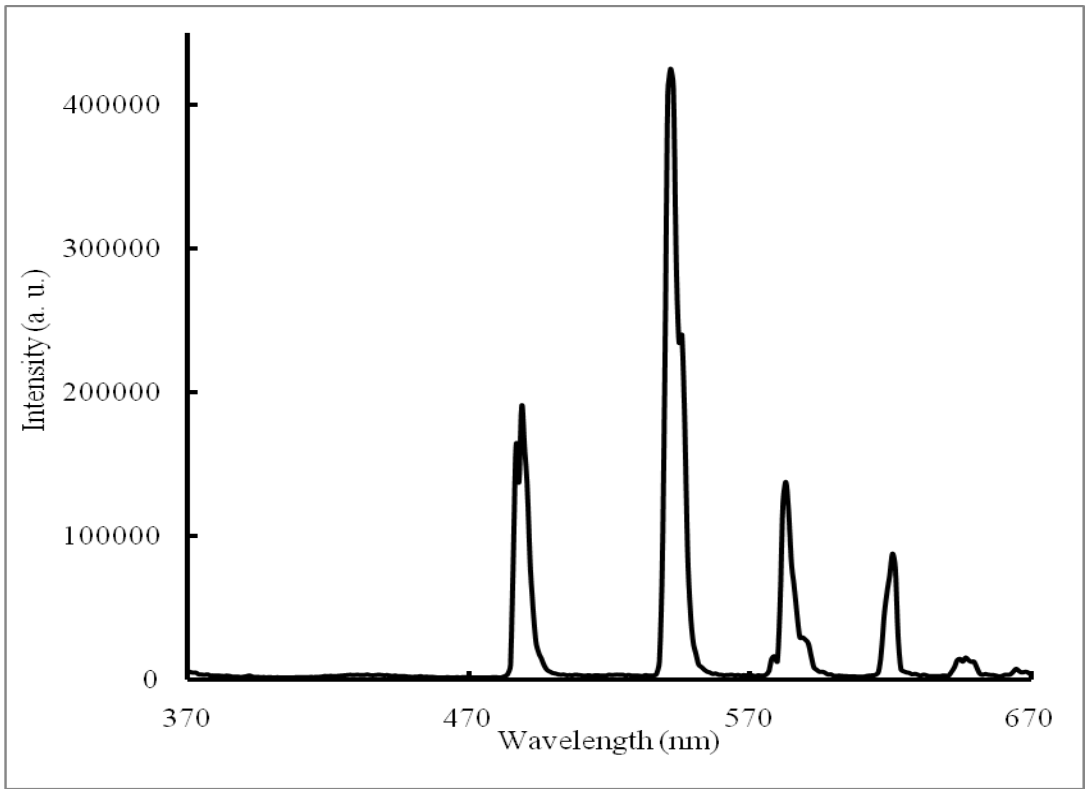

Figure 3.10. Emission spectrum of 4 at liquid N_2 temperature monitored at excitation of 352 nm and emission range of 370-680 nm.

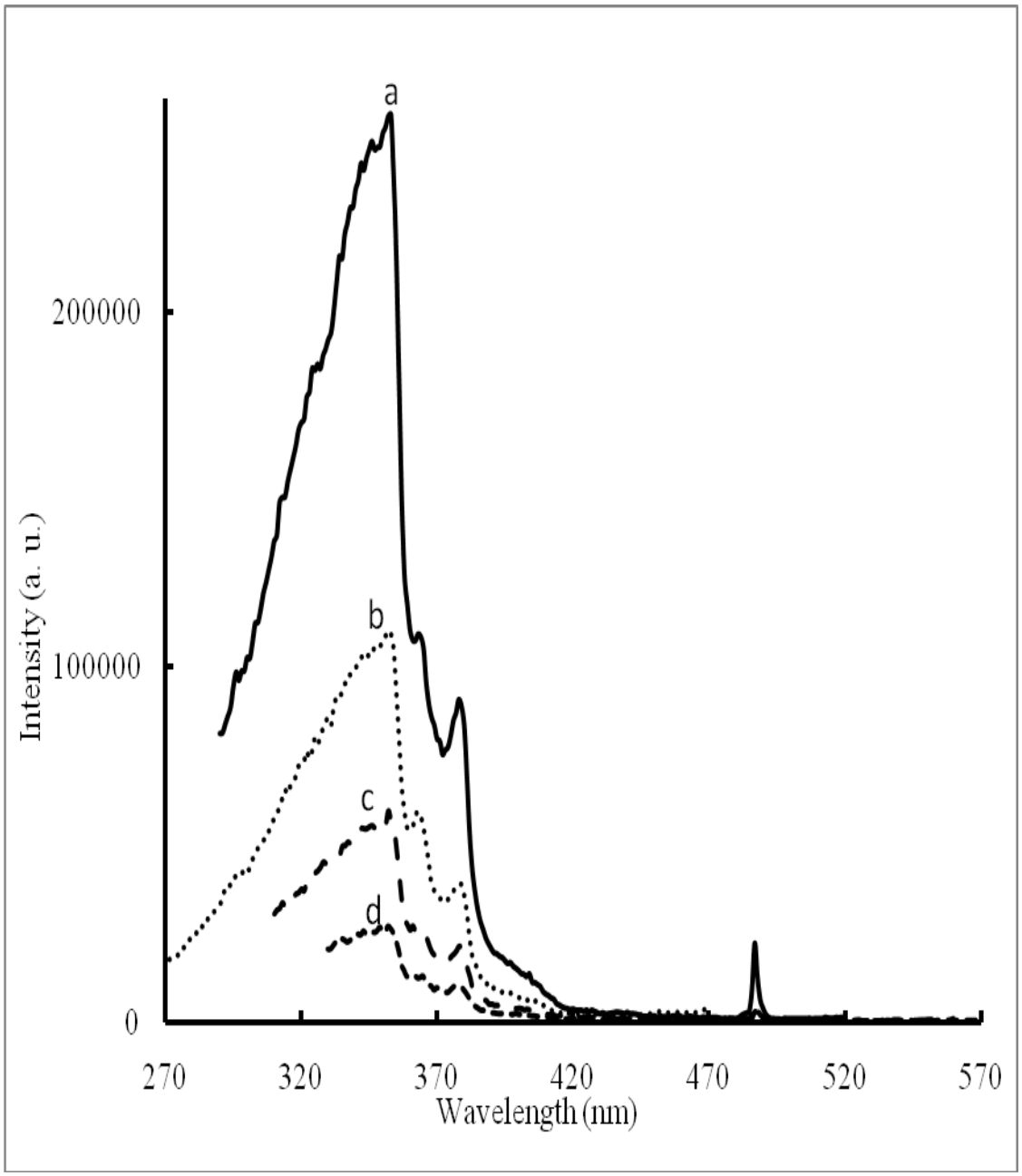

Figure 3.11. Excitation spectra of 4 at liquid N_2 monitored at the emission of (a) 542 nm; (b) 488 nm; (c) 582 nm; and (d) 620nm. These spectra were conducted at liquid N_2 temperature.

The emission and excitation of **4** at room temperature are shown in Figures 3.12 and Figure 3.13. The spectral profile at liquid N_2 is comparable to that of the room temperature data. There is a significant difference between the two spectra. At liquid N_2 the spectra are more intense compared to that of the room temperature.

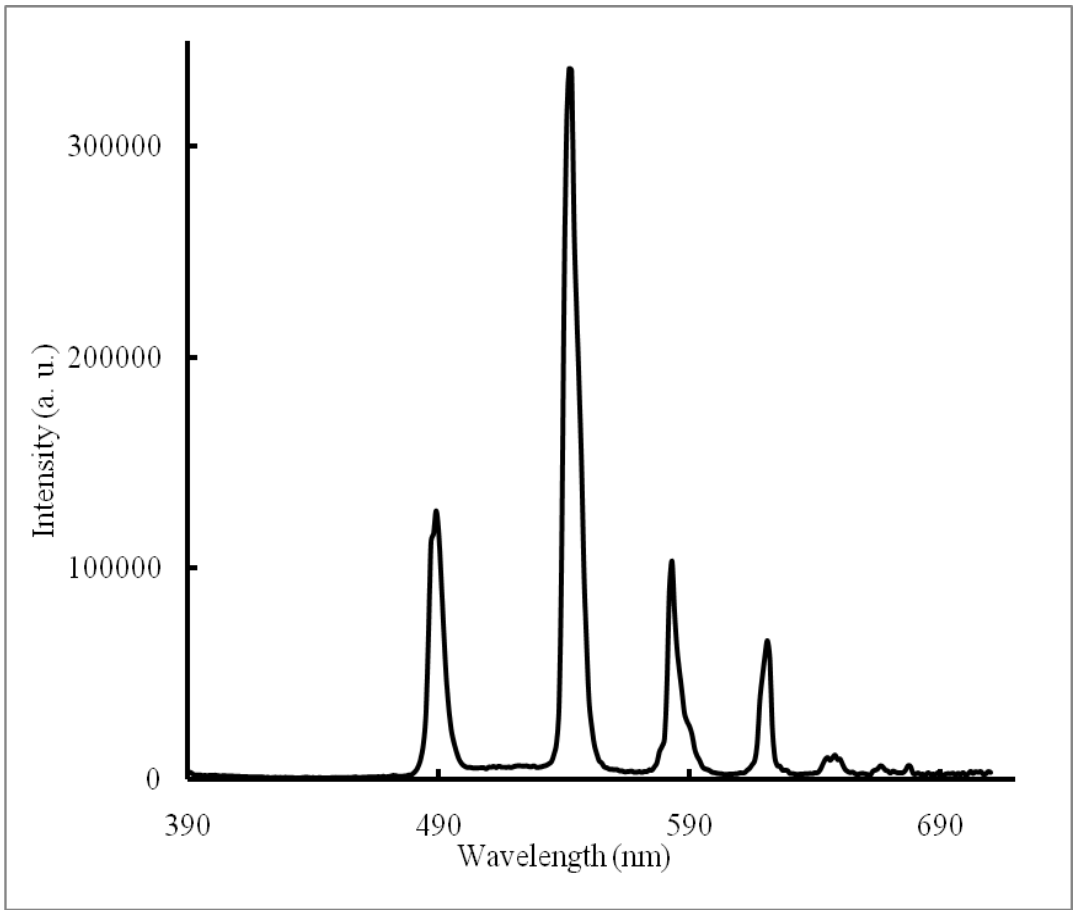

Figure 3.12. Emission spectrum of 4 at room temperature in the range of 390-710 nm. Excitation wavelength used was 366 nm.

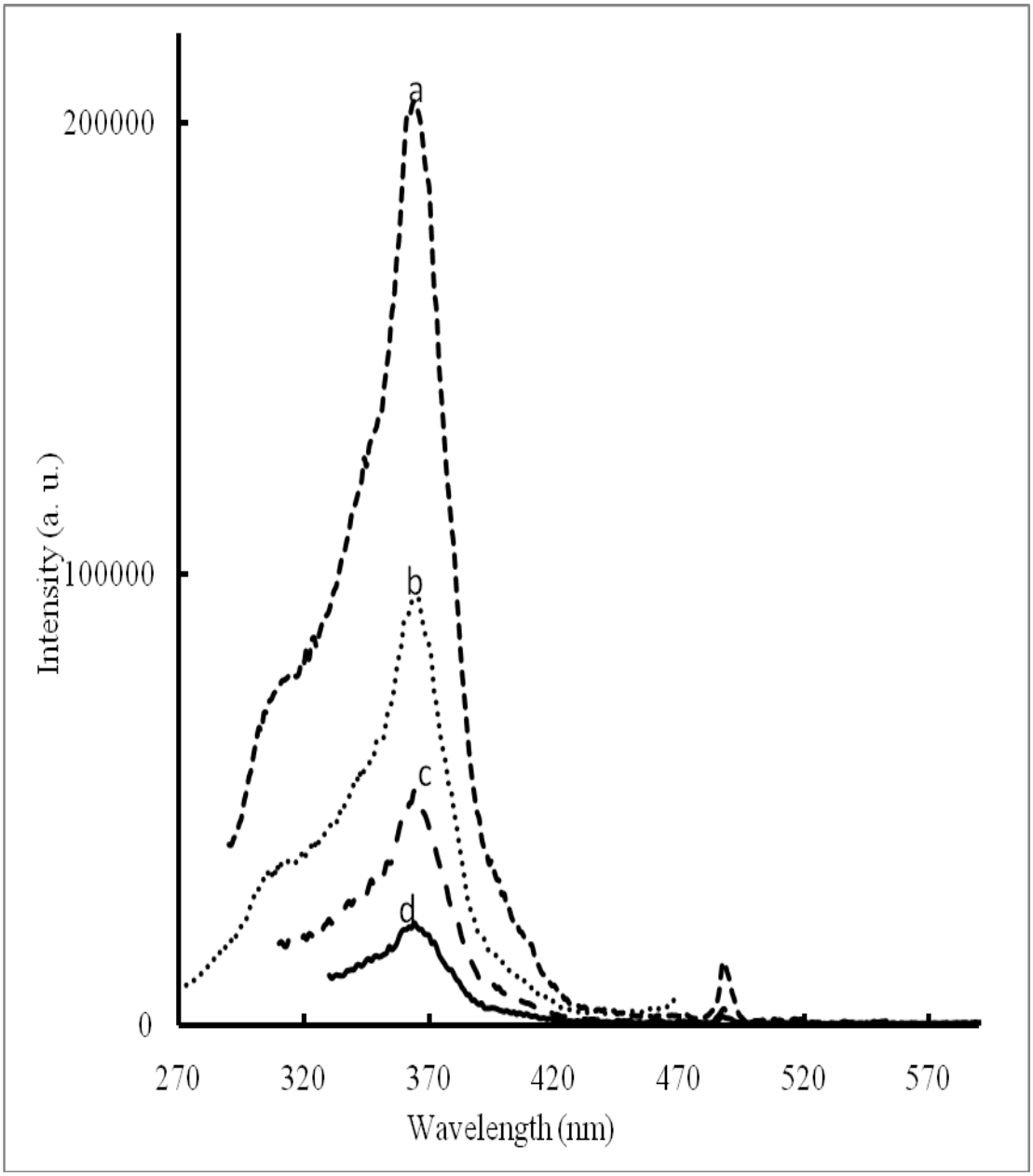

Figure 3.13. Excitation spectra of 4 at room temperature monitored at the emissions of: (a) 542 nm; (b) 488 nm; (c) 583 nm; and (d) 620 nm.

There are four dominate peaks (352, 363, 378, and 487 nm) in the liquid N_2 spectra. In contrast, the result at room temperature consists of a broad dominate band at 360 nm, a sharp band at 486 nm, and a shoulder at the shorter wavelength region between 291-314 nm. Compared to the emission spectra, there are several differences in the excitation spectra at liquid N_2 and room temperature. Although the peaks at liquid N_2 are more intense and more defined, emission is observed at the same wavelengths in both spectra.

There is the presence of f-f transitions at both temperatures in **4**. The emissions at 488, 542, 582, 620, 643, 663, and 673 nm represent $^5D_4 \rightarrow {}^7F_J$ (J = 6, 5, 4, 3, 2, 1) respectively. There is the existence of a strong excited state energy transfer between the donors (terpy and TCP) and the acceptor Tb^{3+} ion because of the observance of the Tb^{3+} emission upon excitation of **4**. These findings are consistent with the interpretation of compounds **1, 2,** and **3** where energy transfer to the acceptor Tb^{3+} ions proceeds efficiently through quenching of donors (terpy and TCP) emission. Direct experimental evidence for the presence of energy transfer in the system is attained when the donor groups show strong excitation upon monitoring the acceptor Tb^{3+} emission.

3.5. Photoluminescence Studies of $[Tb(C_{15}H_{11}N_3)(H_2O)_3]_2(Pt(CN)_4)_3 \cdot 2H_3O$ (5)

The spectra of **5** at liquid N_2 and room temperature are compared in Figures 3.14-3.17. The emission spectrum in Figure 3.14 was collected at liquid N_2 and shows peaks at 488, 541, 582, 619, 646, 662, and 674 nm. At this emission, there are peaks at 345, 356, 369, and 486 nm along with a shoulder between ~393-412 nm. However, spectrum of **5** at

room temperature shows a small red shifting to 544 from 542 nm, although the other peaks remained unchanged. The Figure 3.15a and 3.14a excitation spectra were monitored at the main emission peak at ~544 nm. There is a not much similarity between the excitation spectra of **5** compared at liquid N_2 and ambient temperature. At liquid N_2 the spectra are more intense and defined compare to room temperature. Figure 3.15a shows peaks at 345, 356, 369, 486 nm and a shoulder at ~393-412 nm.

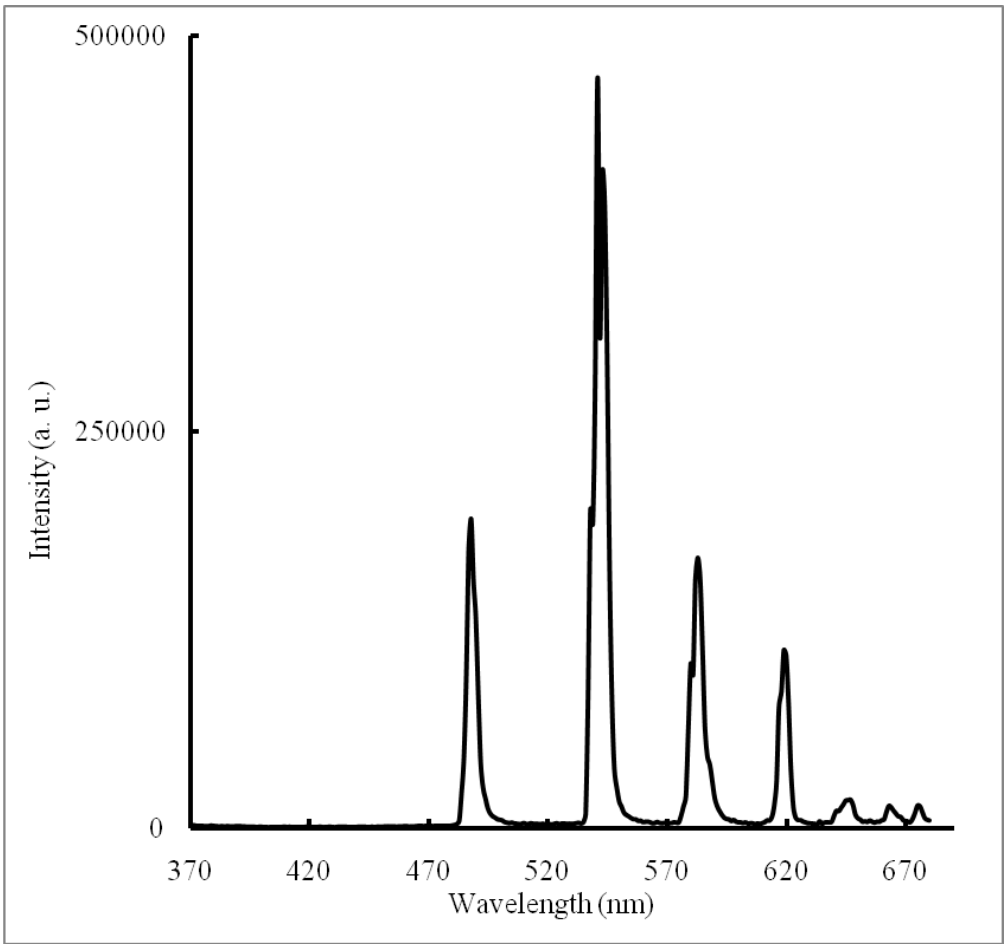

Figure 3.14. Emission spectrum of 5 at liquid N_2 temperature in the 370-680 nm range. The excitation wavelength is 352.

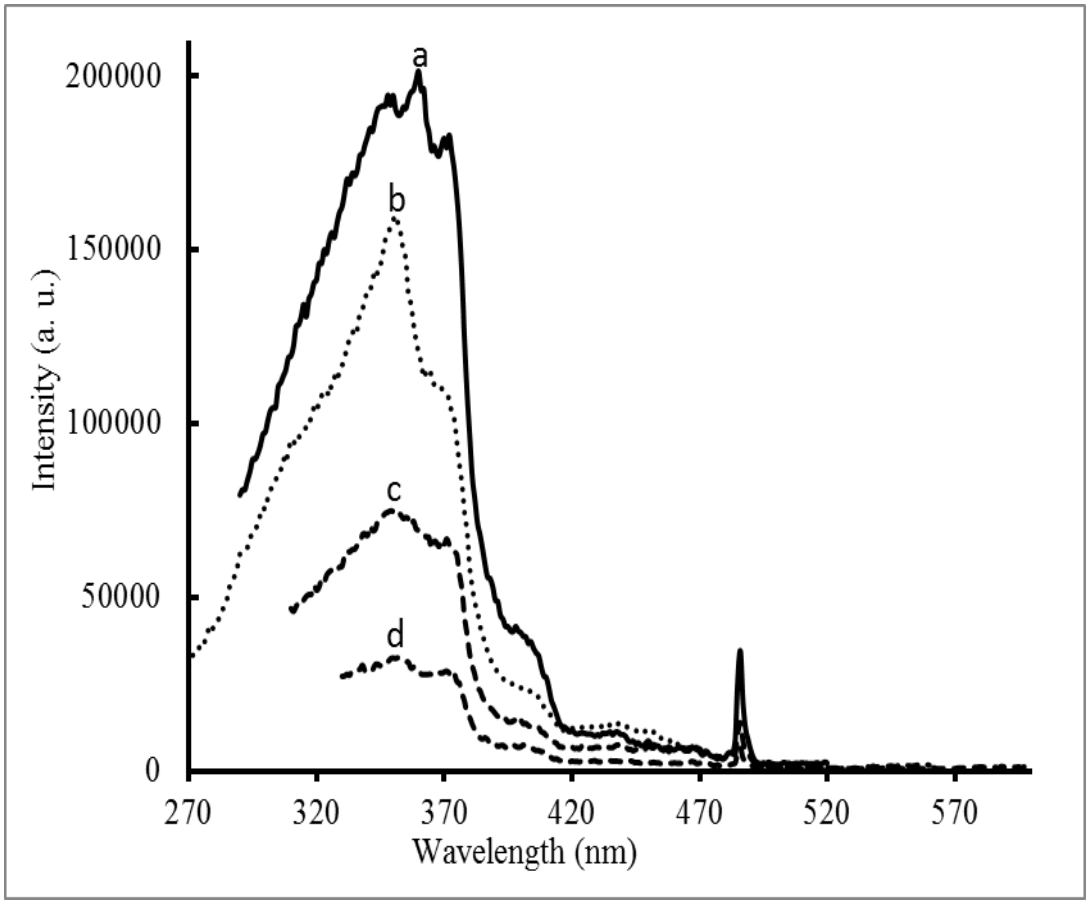

Figure 3.15. Excitation spectra of 5 at liquid N_2 temperature monitored at the emission of: (a) 542 nm; (b) 488 nm; (c) 582 nm; and (d) 618 nm.

The room temperature spectra of **5** are shown in Figure 3.16 (emission) and Figure 3.17 (excitation). The emission spectrum in Figure 3.16 was collected at room temperature and shows peaks at 488, 541, 582, 619, 646, 662, and 674 nm. The excitation spectra (Figure 3.17) contain shoulders at the shorter wavelength (~292-316 nm), and peaks at 361 and 486 nm. These sharp peaks are evidence of f-f transition of Tb^{3+} ion. As a result, there is the existence of energy transfer within the system.

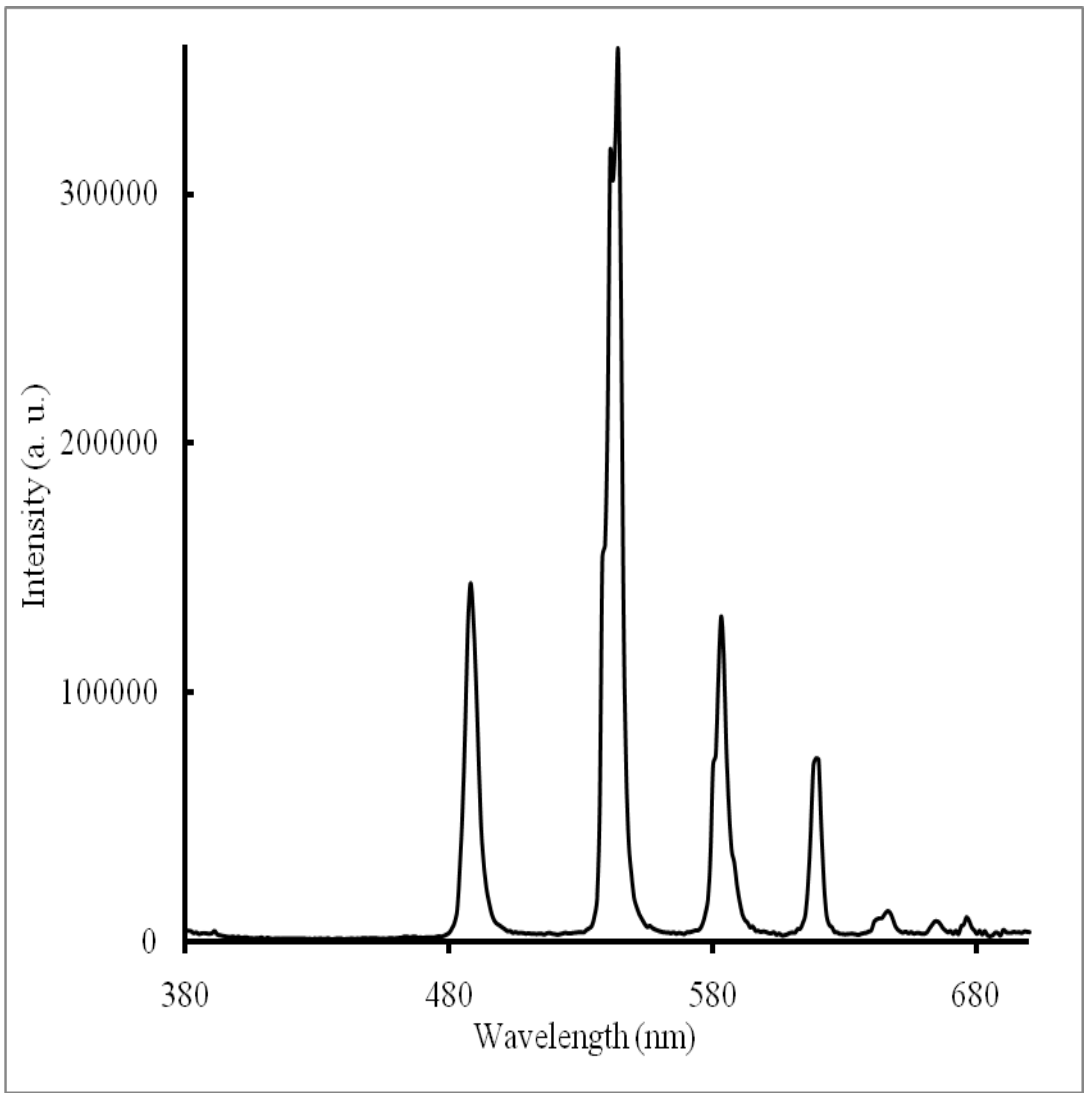

Figure 3.16. Emission spectrum of 5 at room temperature monitored at the excitation of 360 nm, with an emission range of 380-700 nm.

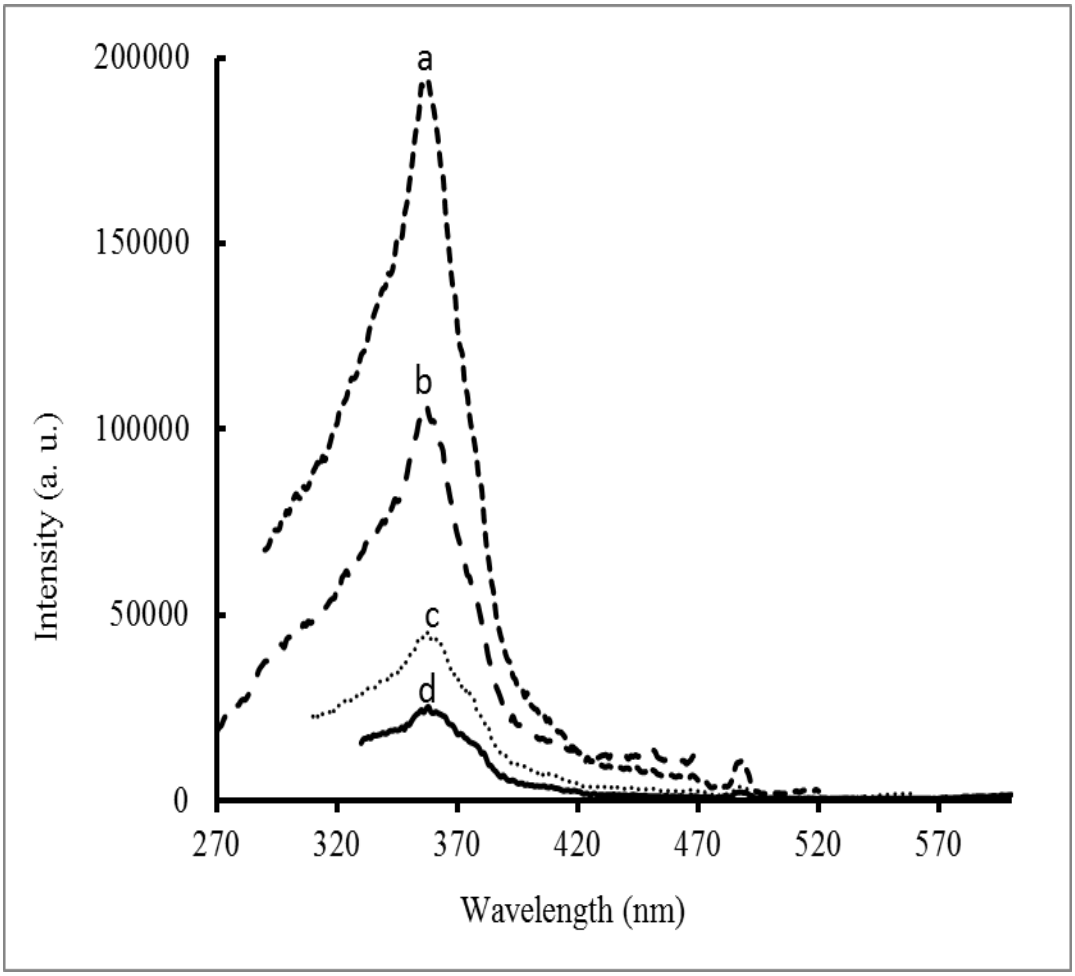

Figure 3.17. Excitation spectra of 5 at room temperature monitored at: (a) 544 nm; (b) 488 nm; (c) 582 nm; and (d) 619 nm.

Compared to **4**, there is the presence of f-f transitions in **5** at both temperatures. The emissions at 488, 542, 582, 620, 643, 663, and 673 nm correspond to $^5D_4 \rightarrow {}^7F_J$ (J = 6, 5, 4, 3, 2, 1), respectively. The observance of the Tb^{3+} emission upon excitation of **5** lead to the conclusion that there is the existence of a strong excited state energy transfer between the donor $Pt(CN)_4^{2-}$ anion and the acceptor Tb^{3+} ion. Like **4,** the evidence of

energy transfer in **5** is demonstrated when the donor groups reveal strong excitation bands upon monitoring the acceptor Tb^{3+} ion emission. There is a strong similarity between **4** and the previous cases **1** and **2** presented where energy is transfer to the acceptor ion by efficiently quenching donor emission from the $Pt(CN)_4^{2-}$ anion.

3.6. Photoluminescence Studies of $Tb(C_{15}H_{11}N_3)(H_2O)(NO_3)_2(Ag(CN)_2)$ (6)

Like the spectra of **4** and **5**, emission spectra of compound **6** which are shown in Figures 3.18 (liquid N_2 temperature) and Figure 3.20 (room temperature) have characteristic f-f bands at 488 nm, 542 nm, 582 nm, 620 nm, and a broadband that maximizes at ~648 nm, along with minor peaks at 667 nm, and 677 nm at both liquid N_2 and room temperatures. Excitation spectra were collected by monitoring the emission at the four major emission peaks. When monitored at the 542 nm emission, the excitation spectra at liquid N_2 shows peaks at 352, 363, and 378 nm and 486 nm. In Figure 3.21 is shown the excitation spectra of compound **6** at room temperature, where peaks at 364 and 488 nm along with a shoulder at ~310 nm are clearly evident of Tb^{3+} transitions.

The excitation spectra at both temperature lack comparison in feature. At liquid N_2 the spectra (Figure 3.19) are more explicit and intense compare to room temperature. The room temperature spectra which are Figure 3.20 contain sharp peaks along with shoulders between 294-315 nm. There is evident of f-f transition bands from the Tb^{3+} ion because of the presence of sharp peaks.

Similarities are observed between the emission of **6** and with **4** and **5.** Similar to **4** and **5,** compound **6** has f-f transitions which are assigned to $^5D_4 \rightarrow {}^7F_J$ (J = 6, 5, 4, 3, 2,

1) transitions. The observance of the Tb^{3+} emission upon excitation of **6** originates from its structural characteristic like in **4** and **5**. There is a direct connection between the acceptor Tb^{3+} ion and donor $Pt(CN)_4^{2-}$ anion, as a result of this feature the acceptor emits strongly when **6** is excited. There is also the existence of a strong excited state energy transfer between the terpy ligand and the Tb^{3+} ion in these systems. The resulting data from **6** lead to the conclusion that energy is transferred to the acceptor ions by efficiently quenching donor emission from the $Pt(CN)_4^{2-}$ anion as stated before in the other systems.

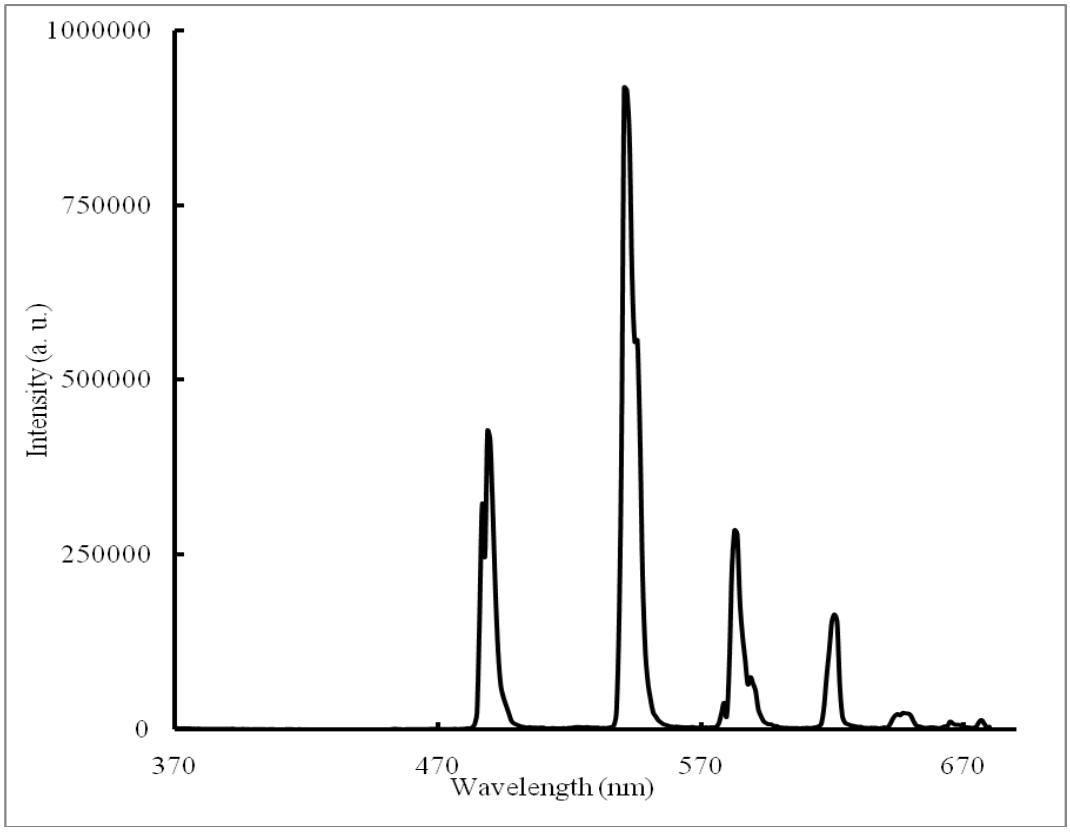

Figure 3.18. Emission spectrum of 6 at liquid N_2 excited at 352 nm, with an emission range of 370-680 nm.

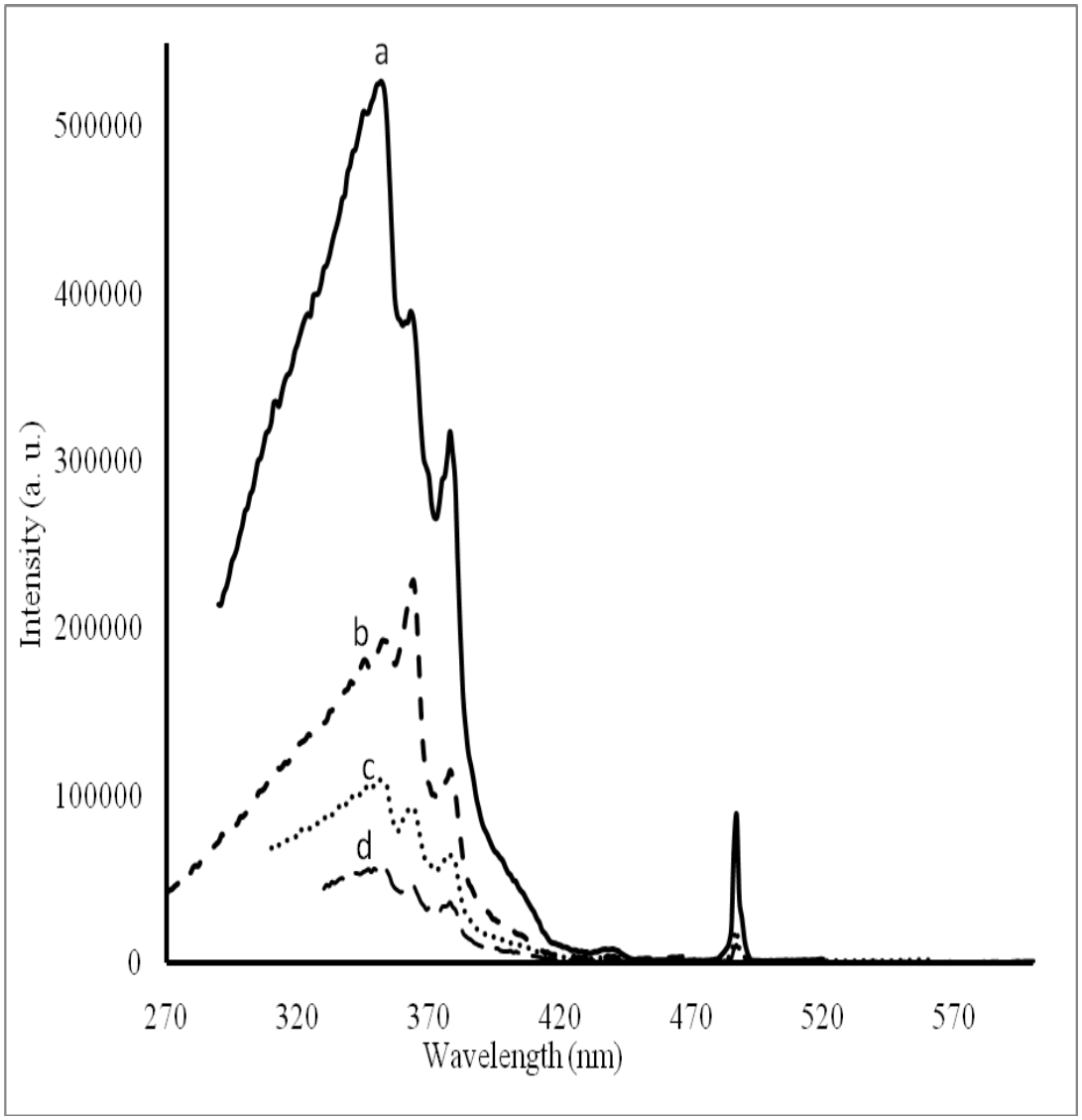

Figure 3.19. Excitation spectrum of 6 at liquid N_2 monitored at the emission wavlengths of: (a) 542 nm; (b) 488 nm; (c) 582 nm; and (d) 620 nm.

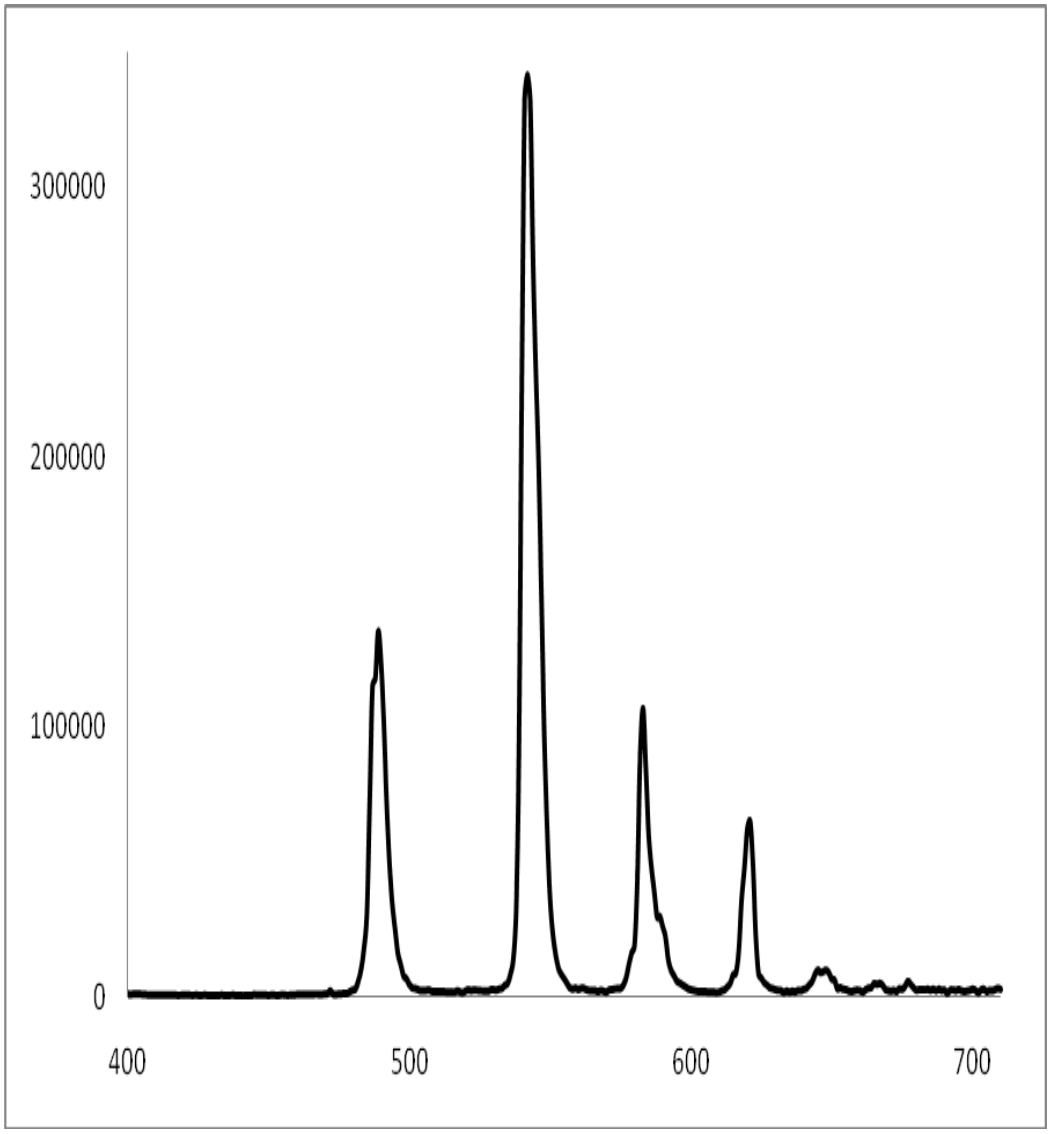

Figure 3.20. Emission spectrum of 6 at room temperature excited with a 366 nm, with an emission range of 390-710 nm.

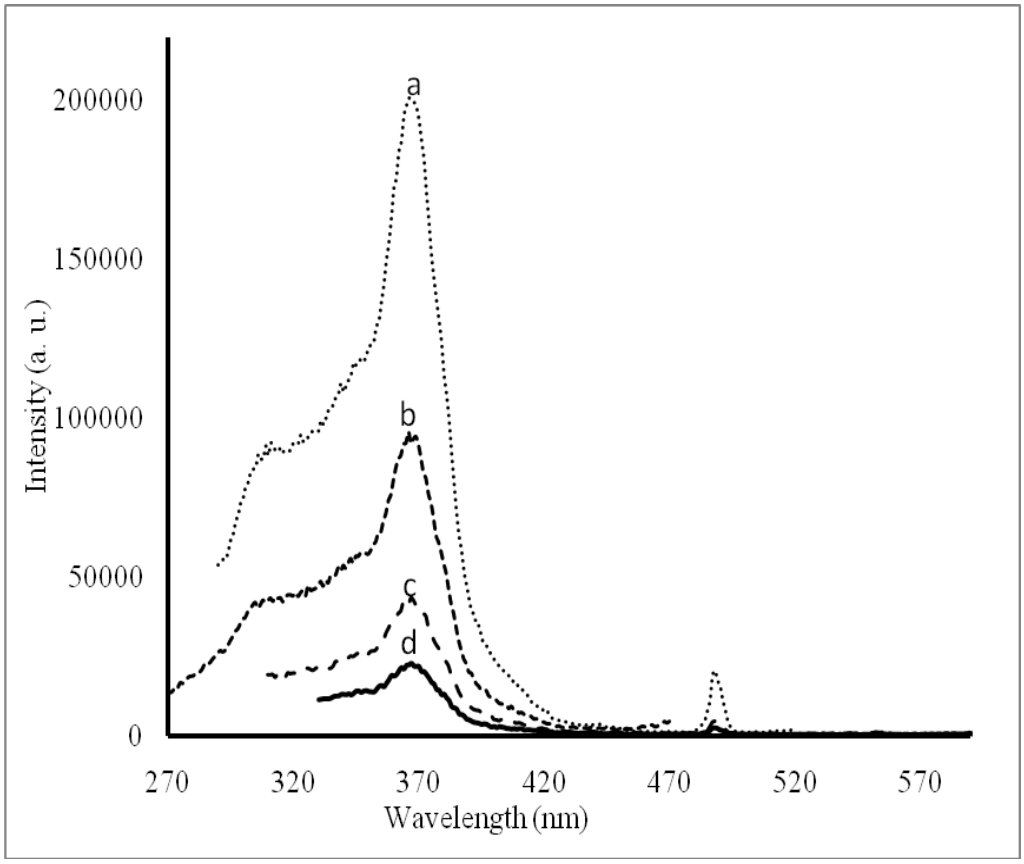

Figure 3.21. Excitation spectra of 6 at room temperature monitored at the emission of: (a) 542 nm, (b) 488 nm; (c) 582 nm; and (d) 620 nm.

3.7. Photoluminescence Studies of $[\{Tb(C_{15}H_{11}N_3)_2(H_2O)_2(CH_3OO)_5\}_2]Pt(CN)_4 \cdot 6H_2O$ (7)

Unlike **4, 5,** and **6**, there is a considerable change in the feature of **7** which lead to the difference in the spectra. Like in the structure of **3,** there is a lack of direct bonding between the acceptor Tb^{3+} ion and the donor $Pt(CN)_4^{2-}$ anion moiety. As a result, the luminescence properties of **5** are altered. Figures 3.22 and 3.23 show the emission of **7** at liquid N_2 and room temperature, respectively.

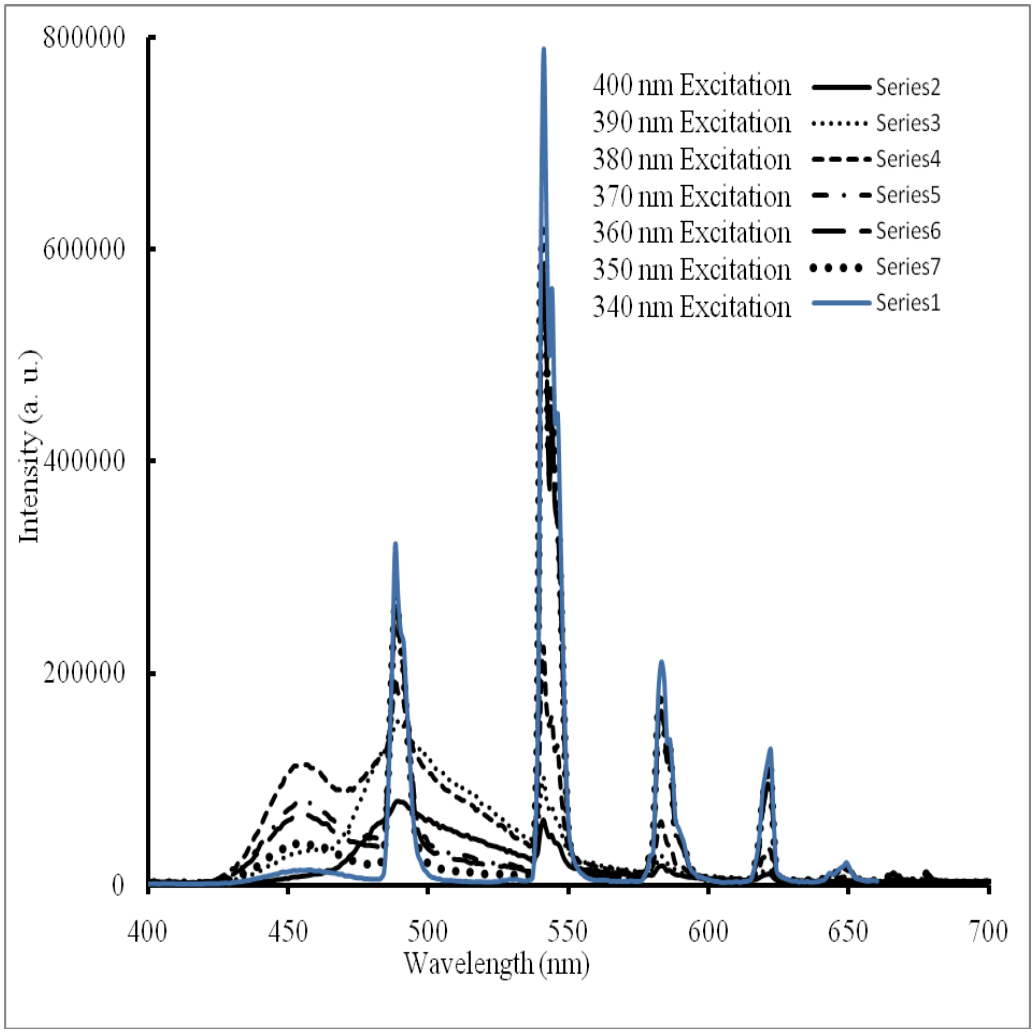

Figure 3.22. Emission spectra of 7 at liquid N_2 resulting from excitation at 340 nm, 350 nm, 360 nm, 370 nm, 380 nm, 390 nm and 400 nm.

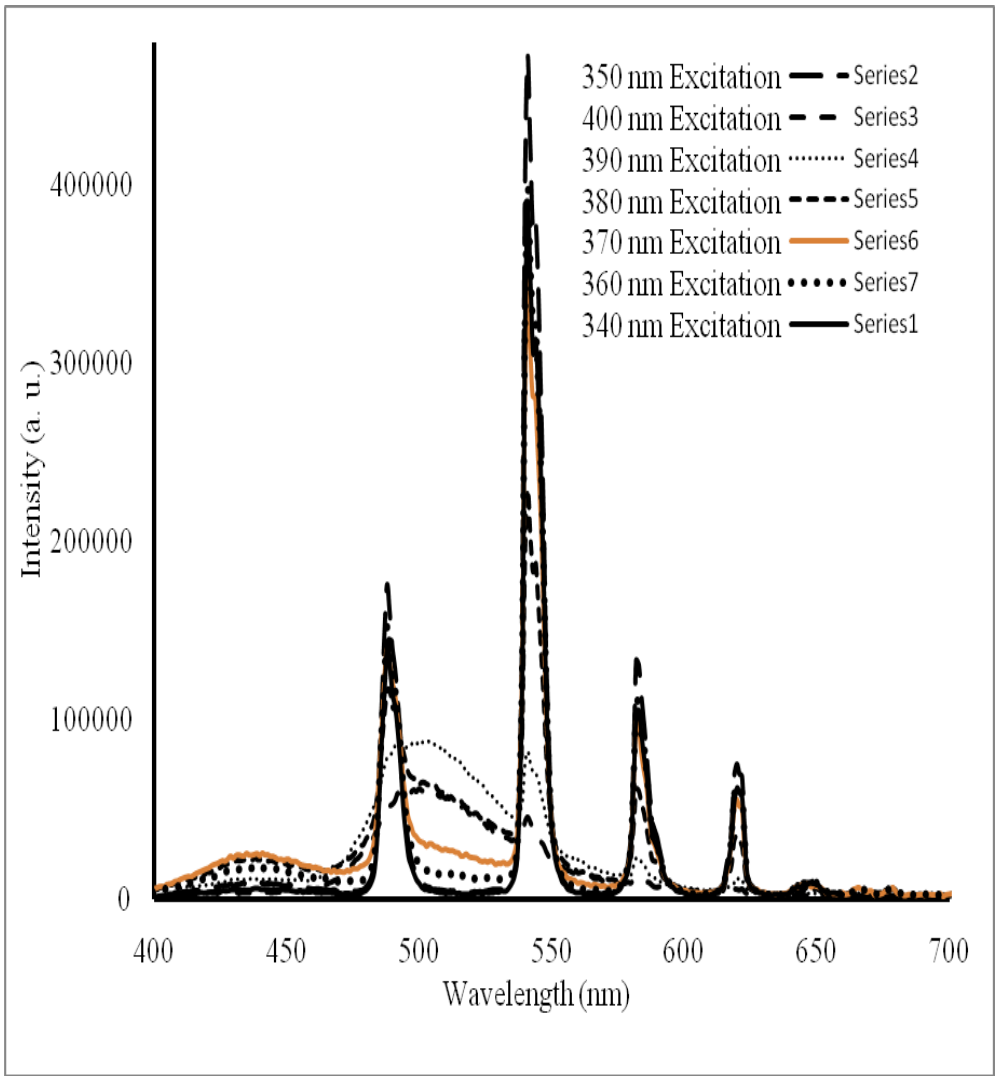

Figure 3.23. Emission spectra of 7 at room temperature collected at various excitation wavelengths.

These spectra were obtained at different excitation wavelengths. The four major peaks at 488 nm, 541 nm, 583 nm, and 622 nm are still present along with broadbands at 456 nm and 500 nm for both temperatures. Compared to the room temperature data, the liquid N_2 spectra are more intense and defined.

Excitation spectra for **7** at liquid N_2 (Figure 3.24) and room temperature (Figure 3.25) were obtained by monitoring the sample at the four major emission peaks. The system shows different spectra when excitation was monitored at the emission of 456 nm and 500 nm. Excitation spectra monitored at 456 nm at liquid N_2 (Figure 3.26a) show peaks at (327 nm, 365 nm, and 380 nm). When monitored at 500 nm peaks at (360 nm, 386 nm, and 434 nm) are observed.

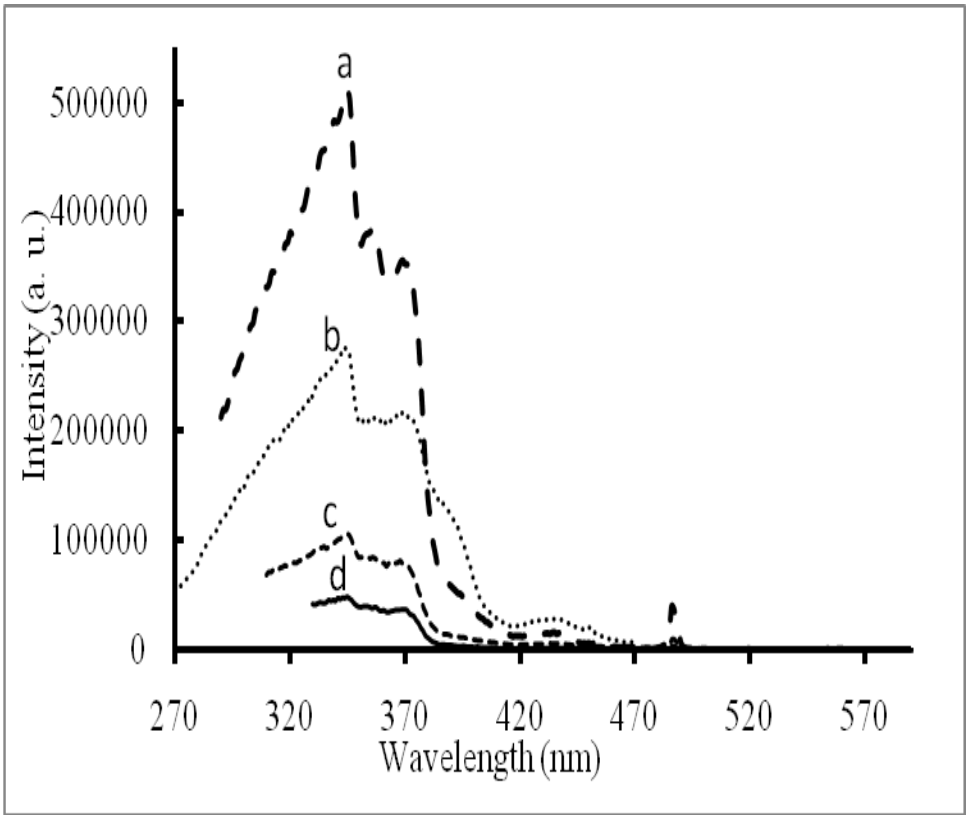

Figure 3.24. Excitation spectra of 7 at liquid N_2 resulting from (a) 541 nm; (b) 488 nm; (c) 583 nm; and (d) 622 nm.

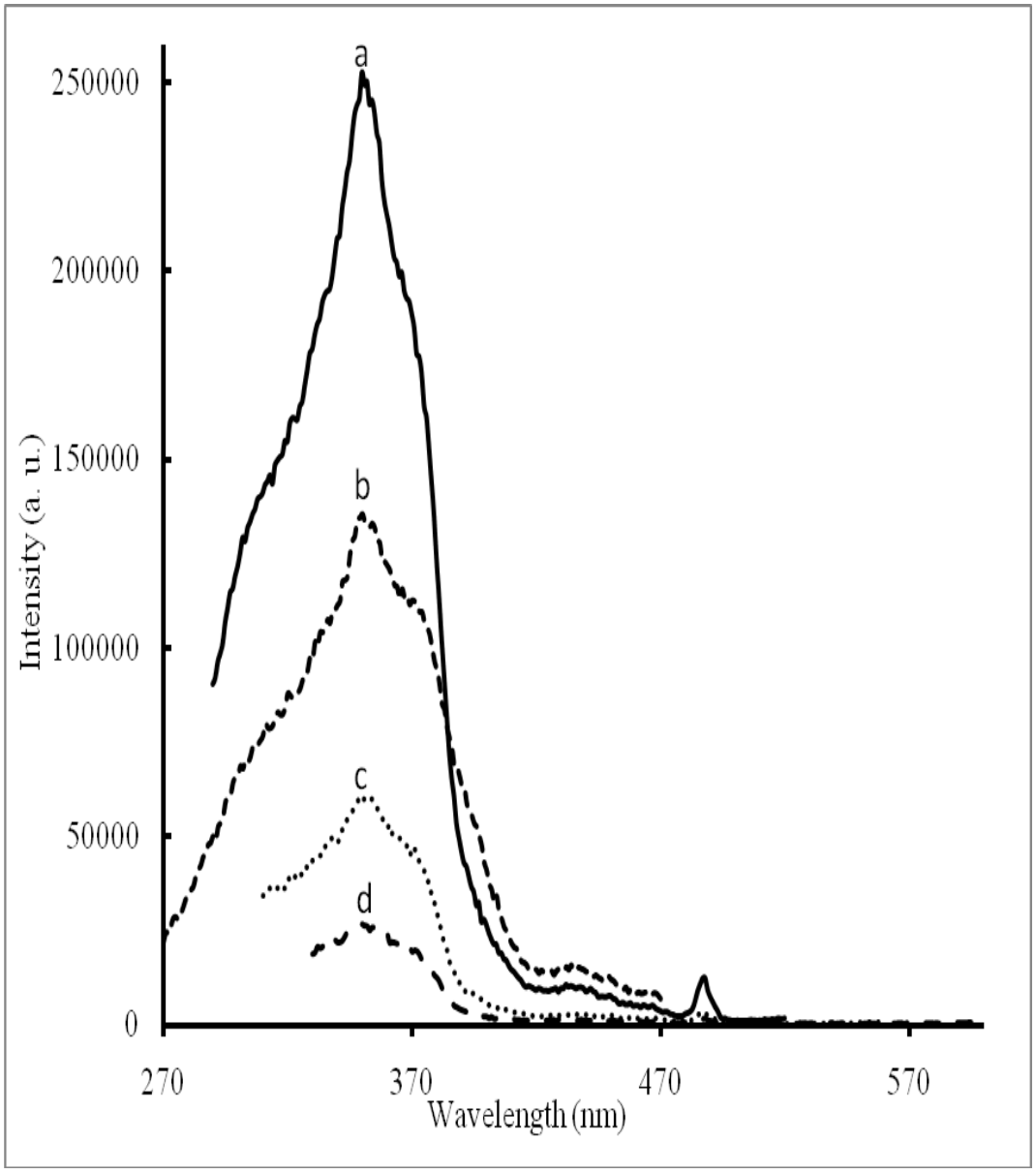

Figure 3.25. Excitation spectra of 7 at room temperature resulting from (a) 542 nm; (b) 488nm; (c) 582 nm; and (d) 620 nm.

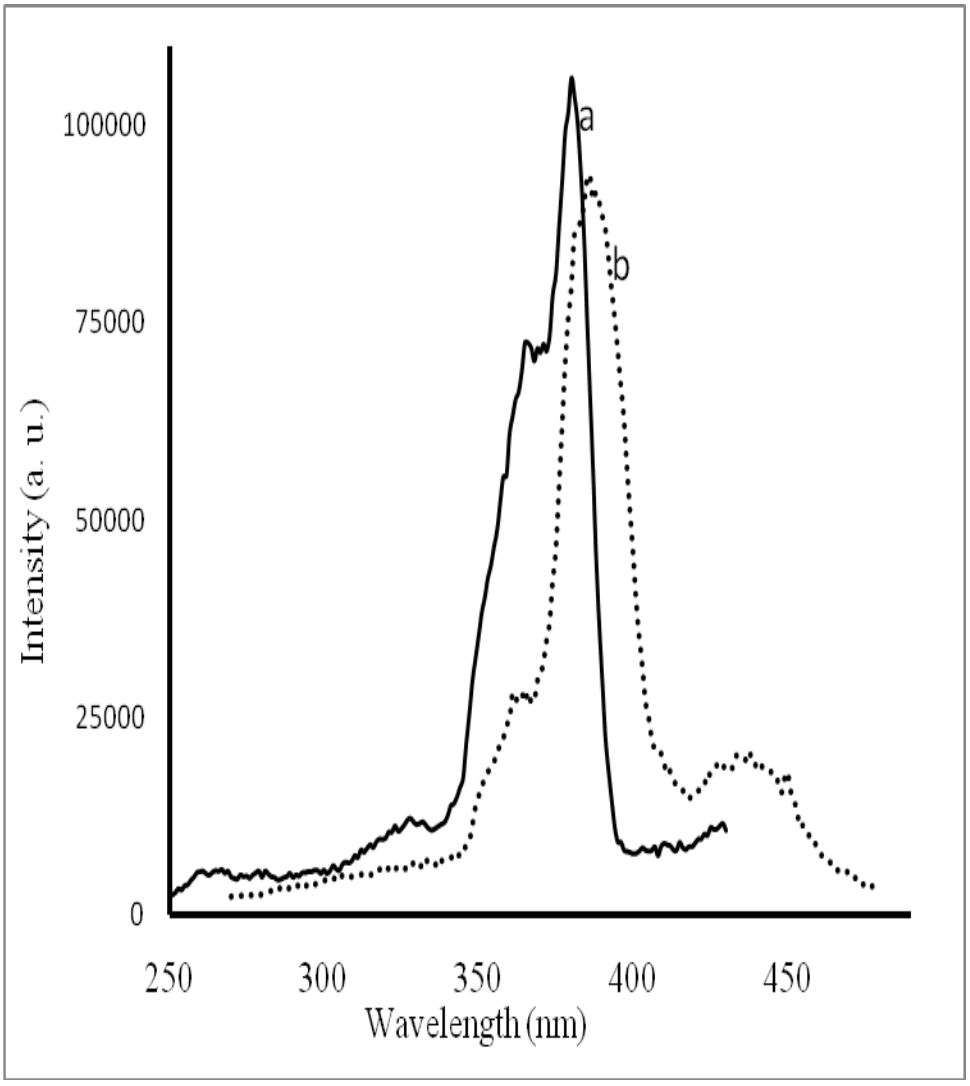

Figure 3.26. Excitation spectra of 7 at liquid N_2 monitored at: (a) 456 nm; and (b) 500 nm.

There is a major change in the spectra at 456 nm and 500 nm at room temperature. When excitation was obtained at 456 nm and the TCP emission of 500 nm at room temperature (Figure 3.27), the spectrum show a broadband between ~350-417 nm with a max at ~389 nm and ~350-400 nm with a max at ~373 nm respectively.

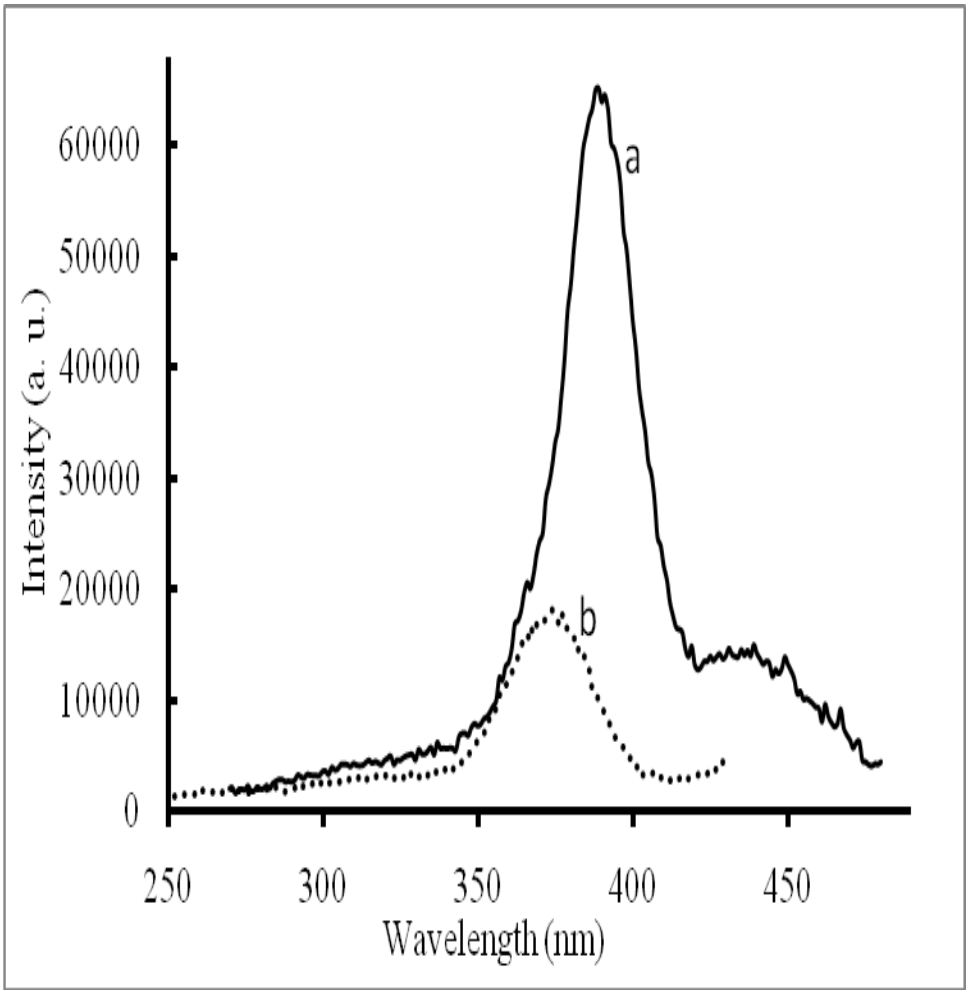

Figure 3.27. Excitation spectra of 7 at room temperature resulting from (a) 456 nm; and (b) 502 nm.

The photoluminescence properties of **7** illustrate significant changes in the emission profiles when the excitation wavelength changes from 340 nm to longer wavelengths. This is because of the lack of direct bonding between the Tb^{3+} ion and the $Pt(CN)_4^{2-}$ group. Like in **3**, the donor/acceptor energy transfer process in **7** is affected as a result of the structural change compared to **1**, **2**, **4**, **5**, and **6**. At 340 nm excitation, a weak

broad emission appear at ~456 nm, and its intensity increases systematically with an increase in the excitation wavelength, but decreases as the system approaches 400 nm achieving a maximum intensity at ~380 nm excitation. Figure 3.28 shows the dependence of the ratios of the emission intensities on excitation wavelength of **7** at liquid N_2 temperature.

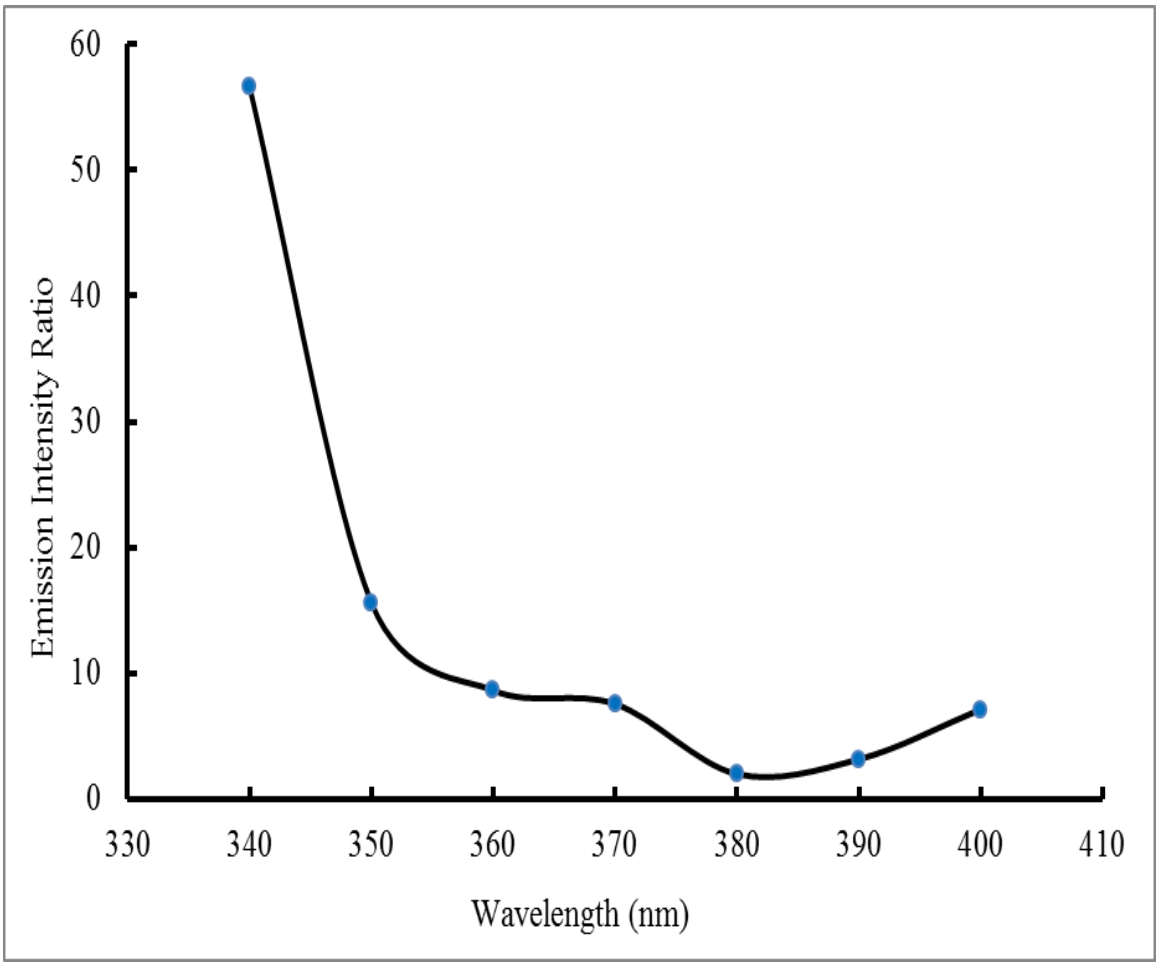

Figure 3.28. Dependence of the emission intensity ratio (541:456 nm) on excitation wavelength for 7.

The characteristics of Tb^{3+} are recognizable in the emission spectra at both temperatures. Compare to **3**, there is the occurrence of an excited state energy transfer between the terpy ligand and the Tb^{3+} ion because of the observance of the Tb^{3+} emission upon excitation at wavelength that are lesser than 340 nm. Opposite to **4**, **5**, and **6**, the energy transfer process decreases in **7** because of the drop in the excitation band when **7** is excited at wavelength greater than 340 nm. As a result, the Tb^{3+} emission decreases as the excitation wavelength move towards a longer wavelength. Nevertheless, there is still the existence of Tb^{3+} transitions, as evidenced by the emission bands at 488, 541, 583, 622, 649, 667, and 678 nm corresponding to $^5D_4 \rightarrow {}^7F_J$ (J = 6, 5, 4, 3, 2, 1), respectively. The terpy group efficiently transfers its excited energy to the Tb^{3+} ion in **7**, but transfer of energy from $Pt(CN)_4^{2-}$ group is altered because of the results obtained.

CHAPTER 4

CONCLUSION

The complexes with nitrate and triflate counter anions display a highly efficient intermolecular energy transfer from dual donors to an acceptor Eu^{3+} and Tb^{3+} ion. Two donor systems played a role in these systems, the organic ligand (terpy) and the platinum tetracyanide ion. Excited energy donors in Compounds **1**, **2, 4, 5,** and **6** display comparable structural features, where a direct coordination between the acceptor (Eu^{3+} and Tb^{3+}) and both donor species is evident. In contrast, in compounds **3** and **7** only the terpy ligand is coordinated while the TCP group exists in the lattice merely as an uncoordinated counter anion. As a result their spectra profiles show significant changes; where in **3** and **7** the sensitization involves only the terpy ligand. A well defined emission band corresponding to the TCP unit is observed signifying the lack of energy transfer from this uncoordinated anion to the acceptor lanthanide ion. Furthermore, all of these complexes show interesting structural features that consist of channels capable of accommodating volatile organic compounds. Studies on VOC sensing by these compounds is currently under evolution in our laboratory.

REFERENCES

1. Omary, M. A.; Patterson, H. H. Luminescence Theory. *Academic Press*, **1999,** 1186 - 207.

2. UV-Vis Luminescence Spectroscopy. http://teaching.shu.ac.uk/hwb/chemistry/tutorials/molspec/lumin1.htm (accessed March 3).

3. Harris, D. C., *Quantitative Chemical Analysis*; Byrd M. L., Ed., and Craig Bleyer: New York, 2007.

4. Skoog, D. A.; Holler, F. J.T.; Nieman, A. *Principles of Instrumental Analysis.* 5th ed. Messina, F., Ed., Harcourt Brace & Company: Orlando, 1998; pp 355 - 76.

5. Skoog, D. A.; Leary, J. J. *Principles of Instrumental Analysis;* 4th ed., Saunders College Publishing: Orlando, 1992; pp 174-93.

6. Electronic Spectroscopy: Theory. http://chemwiki.ucdavis.edu/Physical_Chemistry/Spectroscopy/Electronic_Spectroscopy/Electronic_Spectroscopy%3A_Theory (accessed February 28).

7. Krebs, R. E.; *The history and use of our earth's chemical elements: a reference guide;* Greenwood Publishing Group, Inc.: Westport, 1998, pp 230-4.

8. Binnemans, K. Lanthanide-Based Luminescent Hybrid Materials. *Chem Rev.* **2009,** *109* (9), 4283-374.

9. Richardson, F. S. Terbium(III) and europium(III) ions as luminescent probes and stains for biomolecular systems. *Chem. Rev.* **2002,** *82* (5), 541 - 52.

10. Reifenberger, J. G.; Snyder, G. E.; Baym, G.; Selvin, P. R. Emission Polarization of Europium and Terbium Chelates. *J. Phys. Chem. B* **2003,** *107* (46), 12862 - 73.

11. Vicentini, G.; Zinner, L. B.; Zukerman-Schpector, J.; Zinner, K. Luminescence and structure of europium compounds. *Coordination Chemistry Reviews*, **2000,** *196*, 353 - 82.

12. de Bettencourt-Dias, A. Isophthalato-Based 2D Coordination Polymers of Eu(III), Gd(III), and Tb(III): Enhancement of the Terbium-Centered Luminescence through Thiophene Derivatization. *Inorg. Chem.* **2005,** *44* (8), 2734 - 41.

13. Dutton, P. J.; Conte, L. Terbium Luminescence in Langmuir-Blodgett Films of Octafunctionalized Calix[4]resorcinarenes. *Langmuir* **1998,** *15* (2), 613 - 7.

14. Viswanathan, S.; de Bettencourt-Dias, A. Eu(III) and Tb(III) Luminescence Sensitized by Thiophenyl-Derivatized Nitrobenzoato Antennas. *Inorg. Chem.* **2006,** *45* (25), 10138 - 46.

15. Zhang, H. J.; Fu, L. S.; Wang, S. B.; Meng, Q. G.; Yang, K. Y.; Ni, J. Z. Luminescence characteristics of europium and terbium complexes with 1,10-phenanthroline in-situ synthesized in a silica matrix by a two-step sol-gel process. *Materials Letters*, **1999,** *38*, 260 - 4.

16. Chen, W.; Bovin, J.-O.; Joly, A. G.; Wang, S.; Su, F.; Li, G. Full-Color Emission from In_2S_3 and In_2S_3:Eu^{3+} Nanoparticles. *J. Phys. Chem. B* **2004,** *108* (32), 11927 - 34.

17. Q. Zheng, H. D., M. E. Merritt, C. Malloy, C. Y. Pan, W.-H. Li, , A New Class of Macrocyclic Lanthanide Complexes for Cell Labeling and Magnetic Resonance Imaging Applications. *J. Am. Chem. Soc.* **2005,** *127* (46), 16178 - 88.

18. Maynard, B. A.; Kalachnikova., K.; Whitehead, K.; Assefa, Z.; Sykora,, R. E. Intramolecular Energy Transfer in a One-Dimensional Europium Tetracyanoplatinate. *Inorg. Chem.* **2008,** *47* (6), 1895 - 7.

19. Shunmugam, R.; Tew, G. N. Unique Emission from Polymer Based Lanthanide Alloys. *J. Am. Chem. Soc.* **2005,** *127* (39), 13567 - 72.

20. Lis, S.; Elbanowski, M.; Makowska, B.; Hnatejko, Z. Energy transfer in solution of lanthanide complexes. *Journal of Photochemistry and Photobiology* A: Chemistry, **2002,** *150*, 233 - 47.

21. Giraud, M., Andreiadis, E. S., Fisyuk, A. S., Demadrille, R., Jacques, P., Imbert, D., Mazzanti, M. Efficient Sensitization of Lanthanide Luminescence by Tetrazole-Based Polydentate Ligands. *Inorganic Chemistry* **2008,** *47* (10), 3952 - 4.

22. Galaup, C.; Couchet, J.-M.; Bedel, S.; Tisnes, P.; Picard, C. Direct Access to Terpyridine-Containing Polyazamacrocycles as Photosensitizing Ligands for Eu(III) Luminescence in Aqueous Media. *J. Org. Chem.* **2005,** *70* (6), 2274 - 84.

23. Wang, Q.; Tan, C.; Chen, H.; Tamiaki, H. A New Fluoride Luminescence Quencher Based on a Nanostructured Covalently Bonded Terbium Hybrid Material. *The J. Phys. Chem. C* **2010**, *114* (32), 13879 - 83.

24. Li, Q.; Li, T.; Wu, J. Luminescence of Europium(III) and Terbium(III) Complexes Incorporated in Poly(Vinyl Pyrrolidone) Matrix. *J. Phys. Chem. B* **2001,** *105* (49), 12293 - 6.

25. Petoud, S.; Bünzli, J.-C. G.; Schenk, K. J.; Piguet, C. Luminescent Properties of Lanthanide Nitrato Complexes with Substituted Bis(benzimidazolyl)pyridines. *Inorg. Chem.* **1997,** *36* (7), 1345 - 53.

26. CharbonniÃ¨re, L.; Mameri, S.; Kadjane, P.; Platas-Iglesias, C.; Ziessel, R. Tuning the Coordination Sphere around Highly Luminescent Lanthanide Complexes. *Inorg. Chem.* **2008,** *47* (9), 3748 - 62.

27. Yan, B.; Zhang, H.; Wang, S.; Ni, J. Luminescence Properties of Rare-Earth (Eu^{3+} and Tb^{3+}) Complexes with Paraaminobenzoic Acid and 1, 10-Phenathroline Incorporated into a Lilica Matrix by Sol-Gel Methos. *Materials Research Bulletin*. **1998,** *33* (10), 1517 - 25.

28. Moore, E. G.; Samuel, A. P. S.; Raymond, K. N. From Antenna to Assay: Lessons Learned in Lanthanide Luminescence. *Acc. Chem. Res.* **2009,** *42* (4), 542 - 52.

29. Sato, S.; Wada, M. Realtions between Intramolecular Energy Transfer Efficiencies and Triplet State Energies in Rare Earth β-diketone Chalates. *Bulletin of The Chemical Society of Japan*, **1970,** *43*, 1955 - 62.

30. Raju, G. S. R.; Buddhudu, S.; Rajulu, A. V.; Devi, L. G., Emission Spectra of Tb^3 :PVA Polymer Films. *Spectroscopy Letters: An International Journal for Rapid Communication* **2006,** *39* (5), 487 - 95.

31. Holz, R. C.; Thompson, L. C. Spectroscopically distinct geometrical isomers in a single crystal. Characterization of the eight-coordinate adducts of tris(dipivaloylmethanato) lanthanide(III) with 2,9-dimethyl-1,10-phenanthroline. *Inorganic Chemistry* **2002,** *32* (23), 5251 - 6.

32. Lis, S.; Hnatejko, Z.; Barczynski, P.; Elbanowski, M. Luminescence studies of Eu(III) mixed ligand complexes. *Journal of Alloys And Compounds.* **2002,** 344, 70 - 4.

33. Maynard, B. A.; Smith, P. A.; Ladner, L.; Jaleel, A.; Beedoe, N.; Crawford, C.; Assefa, Z.; Sykora, R. E. Emission Enhancement through Dual Donor Sensitization: Modulation of Structural and Spectroscopic Properties in a Series of Europium Tetracyanoplatinates. *Inorg. Chem.* **2009,** *48* (14), 6425 - 35.

34. Assefa, Z.; Shankle, G.; Patterson, H. H.; Reynolds, R.; Photoluminescence studies of lanthanide ion complexes of gold and silver dicyanides: a new low-dimensional solid state class for nonradiative excited-state energy transfer. *Inorg. Chem.* **1994,** 33 (10), 2187 - 95.

35. Benniston, A. C.; Chapman, G. M.; Harriman, A.; Mehrabi, M. Rostron, S. A. Reversible Luminescence Switching in a Ruthenium(II) Bis(2,2′:6′,2″-terpyridine)-Benzoquinone Dyad. Inorg. Chem. **2005,** *44* (11), 4029 - 36.

36. Benniston, A. C.; Chapman, G. M.; Harriman, A.; Mehrabi, M. Intramolecular Energy Transfer in Molecular Dyads Comprising Free-base Porphyrin and Ruthenium(II) Bis(2,2′:6′,2″-terpyridine) Termini. *J. Phys. Chem. A* **2004,** *108* (42), 9026 - 36.

37.Arena, G.; Calogero, G.; Campagna, S.; Monsu Scolaro, L.; Ricevuto, V.; Romeo, R. Synthesis, Characterization, Absorption Spectra, and Luminescence Properties of Organometallic Platinum(II) Terpyridine Complexes. *Inorg. Chem.* **1998,** *37* (11), 2763 - 9.

38. Benniston, A. C.; Harriman, A.; Pariani, C.; Sams, C. A. Competition between Energy Transfer and Interligand Electron Transfer in Porphyrinâˆ’Osmium(II) Bis(2,2′:6′,2″-terpyridine) Dyads. *J. Phys. Chem. A* **2007,** 111 (37), 8918 - 24.

39. Spence, T. G.; Trotter, B. T.; Posey, L. A. Influence of Sequential Solvation on Metal-to-Ligand Charge Transfer in Bis(2,2′,2″-terpyridyl)iron(II) Clustered with Dimethyl Sulfoxide. *J. Phys. Chem. A* **1998,** *102* (40), 7779 - 86.

40. Benniston, A. C.; Harriman, A.; Li, P.; Sams, C. A. Temperature-Induced Switching of the Mechanism for Intramolecular Energy Transfer in a 2,2′:6′,2″-Terpyridine-Based Ru(II)-Os(II) Trinuclear Array. *J. Am. Chem. Soc.* **2005,** *127* (8), 2553 - 64.

41. Chapman, R. D.; Loda, R. T.; Riehl, J. P.; Schwartz, R. W. Spectroscopic investigation of the multidentate coordination equilibrium among conformational isomers of tris(2,2', 2''-terpyridyl)europium(III) perchlorate in acetonitrile. *Inorg. Chem*. **2002,** *23* (12), 1652 - 7.

42. Bekiari, V.; Lianos, P. Photophysical Behavior of Terpyridineâˆ’Lanthanide Ion Complexes Incorporated in a Poly(N,N-dimethylacrylamide) Hydrogel. *Langmuir*, **2006,** *22* (20), 8602 - 6.

43. Fink, D. W.; Pivnichny, J. V.; Ohnesorge, W. E. Determination of iron at parts-per-billion levels by quenching of 2,2'2"-terpyridine luminescence. *Anal. Chem.* **2002,** *41* (6), 833 - 4.

44. Loosli, A.; Wermuth, M.; Gudel, H.-U.; Capelli, S.; Hauser, J.; Burgi, H.-B. Crystal Structure and Optical Spectroscopy of $Er_2[Pt(CN)_4]_3 \cdot 21H_2O$ and $Er_2[Pt(CN)_4]_2 \cdot SO_4 \cdot 11.5H_2O$**.** *Inorg. Chem.* **2000,** *39* (11), 2289 - 93.

45. Lechner, A.; Gliemann, G.; Pressure effects on the absorption and emission of tetracyanoplatinates(II) in solution. J. Am. Chem. Soc. **2002,** *111* (19), 7469 - 75.

46. H. Yersin, Riedl, U.; Extreme Pressure-Induced Shifts of Emission Energies in $M[Au(CN)_2]$ and $M_2[Pt(CN)_4]$. Compounds with Low-Dimensional and Metal-Metal Interactions. *Inorg. Chem.* **2002,** *34* (7), 1642-1645.

47. Dillinger, R.; Gliemann, G.; Pfleger, H. P.; Krogmann, K. Temperature, magnetic field, and high-pressure effects on the optical properties of quasi-one-dimensional crystals: ethylenediammonium tetracyanoplatinate(II). I*norg. Chem.* **2002**. *22* (9), 1366 - 9.

48. Leyrer, E.; Zimmermann, F.; Zink, J. I.; Gliemann, G. Triboluminescence, photoluminescence, and high-pressure spectroscopy of tetracyanoplatinate salts. Determination of the pressure at triboluminescent sites. *Inorg. Chem.* **2002,** 24 (1), 102 - 6.

49. Rawashdeh-Omary, M. A.; Larochelle, C. L.; Patterson, H. H. Tunable Energy Transfer from Dicyanoaurate(I) and Dicyanoargentate(I) Donor Ions to Terbium(III) Acceptor Ions in Pure Crystals. *Inorg. Chem*. **2000,** 39 (20), 4527 - 34.